SAND2014-20009

SANDIA REPORT
SAND2014-
Unlimited Release
Printed November 2014

Mechanism of Fusion of Pathogenic Enveloped Viruses with the Endosomal Membrane

Michael S. Kent, Bryan Carson, Susan Rempe, Sadie La Bauve, Juan Vanegas, David Rogers, Briana C. Vernon, Bryce Ricken, Dongmei Ye, Edward Moczdlowski, Aihua Zheng, Margaret C. Kielian

Prepared by
Sandia National Laboratories
Albuquerque, New Mexico 87185 and Livermore, California 94550

Sandia National Laboratories is a multi-program laboratory managed and operated by Sandia Corporation, a wholly owned subsidiary of Lockheed Martin Corporation, for the U.S. Department of Energy's National Nuclear Security Administration under contract DE-AC04-94AL85000.

Issued by Sandia National Laboratories, operated for the United States Department of Energy by Sandia Corporation.

Available to DOE and DOE contractors from
U.S. Department of Energy
Office of Scientific and Technical Information
P.O. Box 62
Oak Ridge, TN 37831

Telephone: (865) 576-8401
Facsimile: (865) 576-5728
E-Mail: reports@adonis.osti.gov
Online ordering: http://www.osti.gov/bridge

Available to the public from
U.S. Department of Commerce
National Technical Information Service
5285 Port Royal Rd.
Springfield, VA 22161

Telephone: (800) 553-6847
Facsimile: (703) 605-6900
E-Mail: orders@ntis.fedworld.gov
Online order: http://www.ntis.gov/help/ordermethods.asp?loc=7-4-0#online

SAND2014-
Unlimited Release
Printed September 2014

Mechanism of Fusion of Pathogenic Enveloped Viruses with the Endosomal Membrane

Michael S. Kent[1], Bryan Carson[1], Susan Rempe[2], Sadie La Bauve[1], Juan Vanegas[2], David Rogers[2], Briana C. Vernon[1], J. Bryce Ricken[1], Dongmei Ye[2], Cathryn Siegrist[1], Ryan Davis[3], Edward Moczdlowski[2], Aihua Zheng[4], Margaret C. Kielian[4]

(1) Bioenergy and Defense Technologies; (2) Nanobiology Department
Sandia National Laboratories
P.O. Box 5800
Albuquerque, New Mexico 87185-MS1349

(3) Biomass Science and Conversion Technologies
Sandia National Laboratories
P.O. Box 969
Livermore, California 94551-MS9291

(4) Department of Cell Biology
Albert Einstein College of Medicine
1300 Morris Park Avenue
Bronx, NewYork 10461

Abstract

Dengue virus is a devastating human pathogen responsible for millions of infections each year. No antiviral therapies for Dengue currently exist, making effective treatment of the virus challenging. Dengue is taken into the cell through endocytosis. Low-pH mediated structural rearrangements of the envelope protein E leads to the formation of fusogenic E trimers that facilitate membrane fusion with late endosomes. The fusion mechanism is not fully understood, but is a key target for inhibiting the viral infection pathway. An important aspect of fusion is the dependence on endosomal membrane composition, and in particular, the requirement of anionic lipids. This study aims to characterize the biophysical reasons for this dependence. The work includes experimental studies and molecular simulations of the interactions of E with lipid membranes. These approaches revealed the structure of E bound to lipid membranes including the depth of its insertion into the membrane and the average angle with respect to the membrane, the fundamental interactions involved, the dependence of adsorption and anchoring energy on membrane composition, the membrane curvature induced upon insertion, and the correlation of the above with fusion efficiency of virus like particles (VLPs) with liposomes. As a part of this work we developed a new biophysical technique to measure the energy for pulling E out of a membrane, and distinguished anchoring (pull-out) and binding energies for this nonequilibrium system. We also developed a modeling approach combining molecular and continuum approaches to provide the first theoretical estimate of the binding energy. Taken together, this work lays the foundation for developing a systematic fundamental understanding of fusion in enveloped viruses that has been elusive to date.

ACKNOWLEDGMENTS

We acknowledge the support of the National Institute of Standards and Technology, U.S. Department of Commerce, in providing the neutron research facilities used in this work.

CONTENTS

1. INTRODUCTION....10

2. EXPRESSION OF E AND PRODUCTION OF VLPS....10
   2.1. Expression of wild type and mutant E....21
   2.2. Expression of wild type and mutant VLPs....23

3. STRUCTURAL STUDIES OF E BOUND TO PC:PG AND PC:PE:CH BILAYERS....23
   3.1 Neutron reflectivity studies of structure of membrane-bound E....23
      3.1.1. Method....24
      3.1.2. Results....24
   3.2 Study of membrane curvature induced by insertion of E....26

4. BINDING, UNBINDING, AND FUSION STUDIES....29
   4.1 Dependence of E binding on lipid composition....29
      4.1.1. Method....29
      4.1.2. Results....30
   4.2 Dependence of E unbinding on lipid composition....33
      4.2.1. Method....34
      4.2.2. Results....37
   4.3 Dependence of VLP binding on lipid composition....38
      4.3.1. Method....38
      4.3.2. Results....38
   4.4 Dependence of VLP fusion on lipid composition....40
   4.5 Dependence of VLP binding and fusion on mutations in the fusion loop....43

5. Computational studies....48
   5.1 Combined all-atom simulation and continuum calculation of binding energy....48
   5.2 Simulations of truncated sE binding to free and restrained lipid bilayers....48

6. Attempt to develop a new fusion assay based on flow cytometry....52

7. Attempt to develop a vaccine based on the fusion loop....55

8. SUMMARY....56

6. REFERENCES....60

Distribution....61

FIGURES

Figure 1.1: Organization of DENV structural proteins: (a) Structural proteins C, E, and M shown for a mature virion. Double grey lines represent the lipid bilayer surrounding the capsid, and the black line represents the viral RNA genome. Figure (a) adapted from [5]. (b) Arrangement of E protein dimers on mature virus surface. 90 dimers lay tangential to the lipid membrane and pack in an icosahedral lattice. A single dimer unit is highlighted in the center with a dashed black line. Figure (b) adapted from [8].....11
Figure 1.2: DENV life cycle: Cell-receptor-mediated binding initiates virus internalization. Acidification in the late endosome triggers fusogenic E protein trimer formation enabling membrane fusion. RNA replication and viral budding in the ER are followed by furin cleavage in the TGN. Mature infectious virions are released to the extracellular environment via exocytosis. Figure adapted from [2].....12
Figure 1.3: Soluble E protein structure: (a) 495 residue sequence of E monomer with DI in red, DII in yellow, DIII in blue, and trans-membrane region in blue cross-hatch. (b) Ribbon structure of prefusion E dimer. Domains I, II, and III are indicated, with DI located at the N terminus and the fusion loop located at the C terminus. Figures (a) and (b) adapted from [8]. (c) Ribbon structure of postfusion E trimer. Fusion loops from E monomers cluster to form a hydrophobic fusion tip. Figure (c) adapted from [16].....13
Figure 1.4: Proposed mechanism for membrane fusion: (1) Monomer fusion loop inserted into the target membrane (red). (2) Monomer clustering in the membrane forms fusogenic trimers and negative curvature begins to develop around the fusion loop. (3) DIII folds back towards the fusion loop and the stem region begins to pack against DII, resulting in hemifusion. (4) The stem associates with DII along the full length, achieving fusion and creation of a membrane pore; trimers are in the final postfusion state. Figure adapted from [5].....14
Figure 1.5: Proposed structures for E in association with viral and host membranes. (A) prefusion dimer and post-fusion trimer in association with the viral membrane. (B) Proposed intermediate structure of E upon exposure to low pH in the endosome. The fusion loop is exposed over a timescale of several minutes during which it must insert into the endosomal membrane. Figure adapted from [??].....15
Figure 1.6: Illustration of the binding, insertion, and unbinding of E trimers with lipid membranes along with a conceptual free energy diagram.....16
Figure 2.1: Illustration of the location of the mutations introduced into the fusion loop of E (tip of domain II) in this work.....21
Figure 3.1: Illustration of the tethered lipid bilayer.....24
Figure 3.2. NR data for E bound to 49:21:30 PC:PE:CH tethered lipid bilayer. Also shown are calculated SLD profile and angular distributions for the best fits.....25
Figure 3.3: NR data for E bound to 70:30 PC:PG tethered lipid bilayer. Also shown are calculated SLD profile and angular distributions for the best fits.....26
Figure 3.4: Left panel: Surface pressure versus bulk concentration of sE. Right panel: Total increase in pressure versus bulk concentration of sE.....27
Figure 3.5: X-ray reflectivity for lipid monolayer alone and after increasing the bulk concentration to 3 μM. The shift in the minimum to lower q_z indicates that the lipid layer has slightly increased in thickness.....28

Figure 4.1: Schematic of QCM-D sample chamber: The prepared crystal was placed within the instrument, creating a sealed chamber to hold the liquid sample. 29
Figure 4.2: QCM frequency (F) shift showing adsorption of liposomes to a QCM sensor followed by rupture and fusion. 30
Figure 4.3: QCM frequency changes for sE binding to PC:PG 70:30 lipid bilayers. The binding is partially reversible upon rinsing with buffer after a delay time of 10 min, but is nearly entirely irreversible after a delay time of 100 min. 31
Figure 4.4: QCM frequency changes for sE binding to PC:PE:CH 49:21:30 lipid bilayers. The binding is nearly entirely irreversible after a delay time of only 10 min. 31
Figure 4.5: Comparing QCM results for bilayer compositions 70:30 PC:PG with 49:21:30 PC:PE:Chol. 32
Figure 4.6: QCM frequency changes for bilayer composition 70:30 PC:PE. The adsorption affinity is very low in absence of anionic lipids or cholesterol. 32
Figure 4.7: Comparison of binding levels for membranes with various lipid compositions. The frequency change 30 min after injecting the solution containing sE is plotted for each lipid bilayer composition. 33
Figure 4.8: Illustration of the method used to determine the energy to remove E from a lipid membrane. The grey circles represent liposomes. 35
Figure 4.9: First order rate analysis used to determine the energy to remove E from a lipid membrane. 35
Figure 4.10: Liposome fluorescence measurements: Fluorescent liposomes demonstrate where vesicles migrate within the sucrose gradient for given centrifugation conditions. 70:30 PC:PE and PC:PG with 3% Dansyl-PE were examined at 54,000rpm and 27,000rpm, and time points ranged from 0.25hr to 2.75hr. Centrifugation at 54,000rpm and 27,000rpm required a minimum time of ~0.5hr and ~1hr, respectively, for lipsoomes to fully migrate to the top of the gradient..36
Figure 4.11: Western blot of 12 mM sE + 80:20 PC:PG liposomes, incubated at pH = 3.0 for 4 hr at 20 ºC. The mixture was then loaded onto a gradient and spun for 6 h at 20 ºC. 36
Figure 4.12: Fraction of protein bound to the liposomes as a function of time spinning at 54000 RPM at 20 ºC, 30 ºC, and 40 ºC. The rate constants are given by the slopes of the lines. 37
Figure 4.13: Arrhenius plot of the dependence of the rate constants on inverse temperature. The activation energy for unbinding is determined to be 155 kJ/mol from the slope. This corresponds to 60 +/- 3 kT at 37 ºC. 37
Figure 4.14. QCM data for VLP binding to PC:PG 70:30 lipid bilayers showing the effect of pH, mol% PG in the bilayer, and delay time between lowering the pH and injecting VLPs into the measurement cell containing the lipid bilayer. The right panel shows and expanded view of the first 50 minutes. 39
Figure 4.15: Loss of VLP binding as a function of delay time between lowering the pH and injecting the VLPs into the measurement cell. Left panel: VLP binding after 10 min and 40 min delay times relative to binding after 10 s delay time for VLP concentration of 10.6 nM and pH 5.5. Right panel: VLP binding after 10 min delay time relative to binding after 10 s delay time for pH 5.5 and pH 6.0. 39
Figure 4.16: QCM data for VLP binding to PC:PG 70:30 and PC:PE:CH 49:21:30 lipid bilayers showing the effect of VLP concentration in each case. For each curve the delay time between lowering the pH and injecting VLPs into the measurement cell containing the lipid bilayer was ~ 10 s. 40

Figure 4.17: VLP-liposome fusion assay using DiD labeled VLPs. Optimization of DiD concentration.....41
Figure 4.18: VLP-liposome fusion assay using PC:PG liposomes with a range of PG content. .42
Figure 4.19: VLP-liposome fusion assay using PC:PE:CH 49:21:30 liposomes for concentrations 1x, 3x, and 8x that of the wt. Corresponding data for PC:PG 70:30 are shown in the bottom panel (note the change in the y-axis scale). 42
Figure 4.20: left panel: VLP-bilayer binding using PC:PG 7:3 liposomes and comparing wt and mutant VLPs. Right panel: VLP-liposome fusion assay using PC:PG 7:3 liposomes comparing wt VLPs from different batches.....43
Figure 4.21: Fusion of W101F mutant VLPs with PC:PG 7:3 liposomes. Top panels: mutant VLPs at 8x of conc used for wt VLPs in Figure 4.19. Bottom panels: mutant VLPs at 24x of conc used for wt VLPs in Figure 4.19. The % fusion values obtained by ratio with the value after Triton X addition are given in the legends. 44
.....45
.....45
Figure 4.22: Fusion of K110E mutant VLPs with PC:PG 7:3 liposomes. Top panels: mutant VLPs at 8x of conc used for wt VLPs in Figure 4.19. Bottom panels: mutant VLPs at 24x of conc used for wt VLPs in Figure 4.19. The % fusion values obtained by ratio with the value after Triton X addition are given in the legends. 45
Figure 4.23: Western blot of protein extracted from the mutant VLPs using an antibody for prM. The mutant VLPs are labeled at the top and free prM protein is shown at the right and used for calibration. 47
Figure 4.24: Western blot of E extracted from the mutant VLPs using the antibody for prM (lower bands) and also an antibody for E that binds to domain III far from the locations of the mutations (upper bands). Wt VLPs are shown at the right. 47
Figure 5.1: (Left panel) Side by side comparison of the truncated sE trimer (blue) and the full protein. (Middle) Overlap of the two protein structures after simulating each system for 100 ns. (Right) Structural alignment between the simulated truncated and full monomers. Disulfide bonds shown in yellow. 49
Figure 5.2: (Left) Starting configuration of a membrane simulation with four truncated trimers in contact with the lipid molecules. (Right) Snapshot of the system after simulating for 400 ns. 50
Figure 5.3: Different types of hydrogen-bonding interactions identified between the protein and lipid molecules. 50
Figure 6.1: Light scattering (left panel) and fluorescence (right panel) readouts from a flow cytometer in initial fusion tests involving VLPs with POPC liposomes and POPG liposomes loaded with NBD-rhodamine. 53

NOMENCLATURE

DOE	Department of Energy
NR	Neutron reflectivity
Tris	Trizma buffer
PBS	Phosphate buffer
DV	Dengue virus
E	Envelope protein of Dengue virus
VLP	Virus-like particle
QCM	Quartz crystal microbalance

1. INTRODUCTION

Background and Global Threat of Dengue Virus

Dengue virus (DENV) is considered the most common arbovirus (i.e. arthropod-borne virus) and is currently endemic in more than 100 countries worldwide [1]. Disease transmission occurs by means of a specific mosquito vector (*Aedes aegypti*) prevalent in certain tropic and subtropic environments [2, 7]. As such, DENV is most prevalent in South America, Central America, select countries in Africa, and Southeast Asia, responsible for an estimated 50-100 million cases of infection each year worldwide [1-4, 6]. Of these, an estimated 500,000 cases result in hospitalizations and about 12,500 cases are fatal [6]. Dengue fever (DF) can produce symptoms that range from skin rash, headache, and muscle ache to joint pain and eye redness. More severe symptoms of internal bleeding and excessive fluid loss are associated with Dengue hemorrhagic fever (DHF) and Dengue shock syndrome (DSS). These ailments have the potential to become lethal and are more likely to develop upon secondary DENV infection [19]. Thus, in locations where DENV is rampant, the likelihood of repeat infection and life-threatening illness is greatly increased.

Currently, no antiviral therapies for DENV exist, making effective treatment of the virus challenging. Four different serotypes of the virus exist (DENV 1-4), which contributes to the difficulty in developing effective antiviral therapies for the disease and treating repeat infections. A patient that contracts DENV without having previous exposure will likely experience the symptoms associated with DF and will generally be able to develop an immune response against that particular serotype. However, this immunity is only afforded against that serotype and not the other three available. Since four serotypes exist, the chance of contracting a heterotypic serotype of DENV upon secondary infection is high. Unfortunately, secondary infection leads to complications in a patient's antibody response, which make neutralizing the disease very challenging. It is believed that antibodies developed in response to primary infection actually enhance infection from a different serotype by causing large amounts of chemical mediators to be released from cells. This in turn causes membrane damage, and ultimately, endothelial cell leakage [2]. Heterotypic secondary infection thus promotes DHF and DSS symptoms by compromising cell membrane function.

Structure and Lifecycle of DENV

DENV is a spherical enveloped virus classified in the *Flaviviridae* family, which contains other significant flavivirus pathogens such as West Nile virus (WNV), tick-borne encephalitis virus (TBEV), and yellow fever virus (YFV). Common to flaviviruses is an envelope glycoprotein E that facilitates viral infection by promoting fusion of the viral and host cell membranes [1, 8]. The lipid membrane of the virion encapsulates the positive-sense RNA genome, which is released into the host cell upon fusion and replicated [2, 5]. The organization of a mature virus particle consists of three main structural proteins: the capsid protein (C), membrane protein (prM/M), and envelope protein (E) as shown in Figure 1.1a. The envelope protein is integral to successful infection of a host cell by promoting membrane fusion. Cryo-electron microscopy has revealed that, in the native state, 90 E protein dimers pack in an icosahedral lattice, coating the outside of the virus particle, and lay tangential to the viral

membrane in a head-to-tail fashion [5, 8, 28, 29]. A schematic of this protein organization is shown in Figure 1.1b.

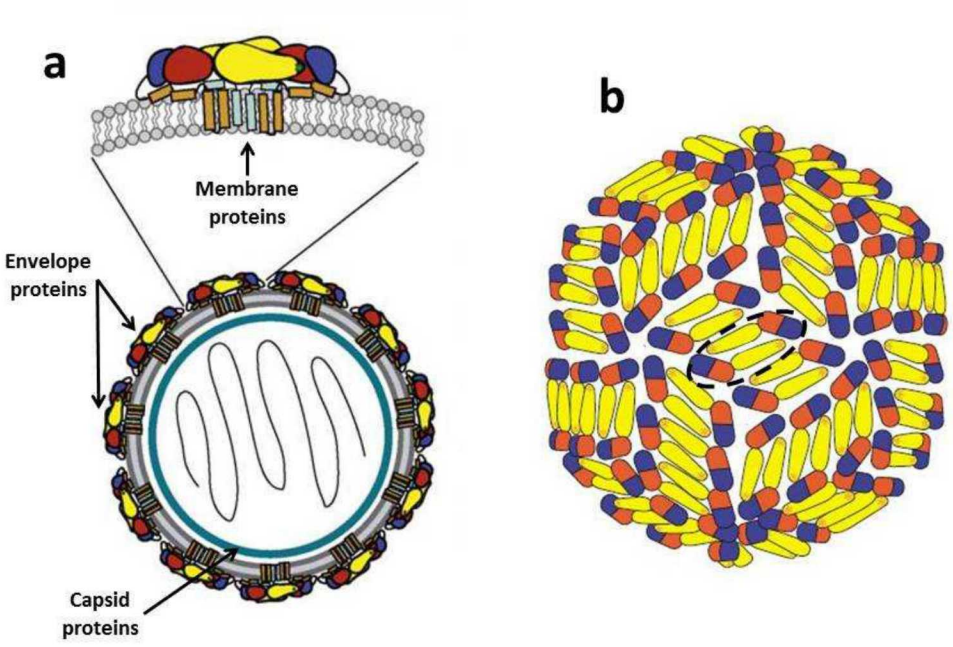

Figure 1.1: Organization of DENV structural proteins: (a) Structural proteins C, E, and M shown for a mature virion. Double grey lines represent the lipid bilayer surrounding the capsid, and the black line represents the viral RNA genome. Figure (a) adapted from [5]. (b) Arrangement of E protein dimers on mature virus surface. 90 dimers lay tangential to the lipid membrane and pack in an icosahedral lattice. A single dimer unit is highlighted in the center with a dashed black line. Figure (b) adapted from [8].

A complete understanding of the infection pathway would aid development of antiviral treatments for DENV. Figure 1.2 depicts the DENV lifecycle from internalization to replication and release. A description of the lifecycle events are as follows: Viral entry into the host cell is initiated when glycoprotein E of the mature virion binds to the surface of the cell via a cell-receptor-mediated interaction. Though E has been identified as the viral component responsible for initial cellular attachment, the exact cellular receptor(s) required for this interaction to take place have not been fully characterized. However, various reports identify a number of receptor molecules that enable DENV virus replication, each dependent upon such factors as the virus serotype and the cultured cell type. This suggests that DENV is able to bind multiple molecules for cell entry [1, 2, 9-11].

After the virus binds to the cell surface, it becomes internalized through endocytic uptake. Once the endosome forms, the internal environment gradually acidifies as the endosome matures, exposing the virus to the low pH environment. This change in pH triggers a conformational rearrangement of E proteins on the surface of the virus, creating fusogenic trimers that facilitate membrane fusion between the viral and endosomal membranes [34, 35].

Membrane fusion releases the nucleocapsid of the virus into the intracellular environment, where the cell's machinery is utilized to replicate the RNA genome and assemble copies of the nucleocapsid. The virus progeny assemble by budding into the endoplasmic reticulum (ER) and are transported through the host secretory pathway [12]. At this point, the virions are considered immature, since E is associated with the prM (pre-membrane) protein complex. Before release at the cell surface via exocytosis, further processing of the prM complex takes place within the Trans-Golgi network (TGN). Here, the pr peptide (used to prevent premature viral fusion during transit through the low pH environment of the TGN) is cleaved by a host-encoded furin protease [3, 20, 21]. The mature infectious virus progeny is then released into the extracellular environment to infect other cells.

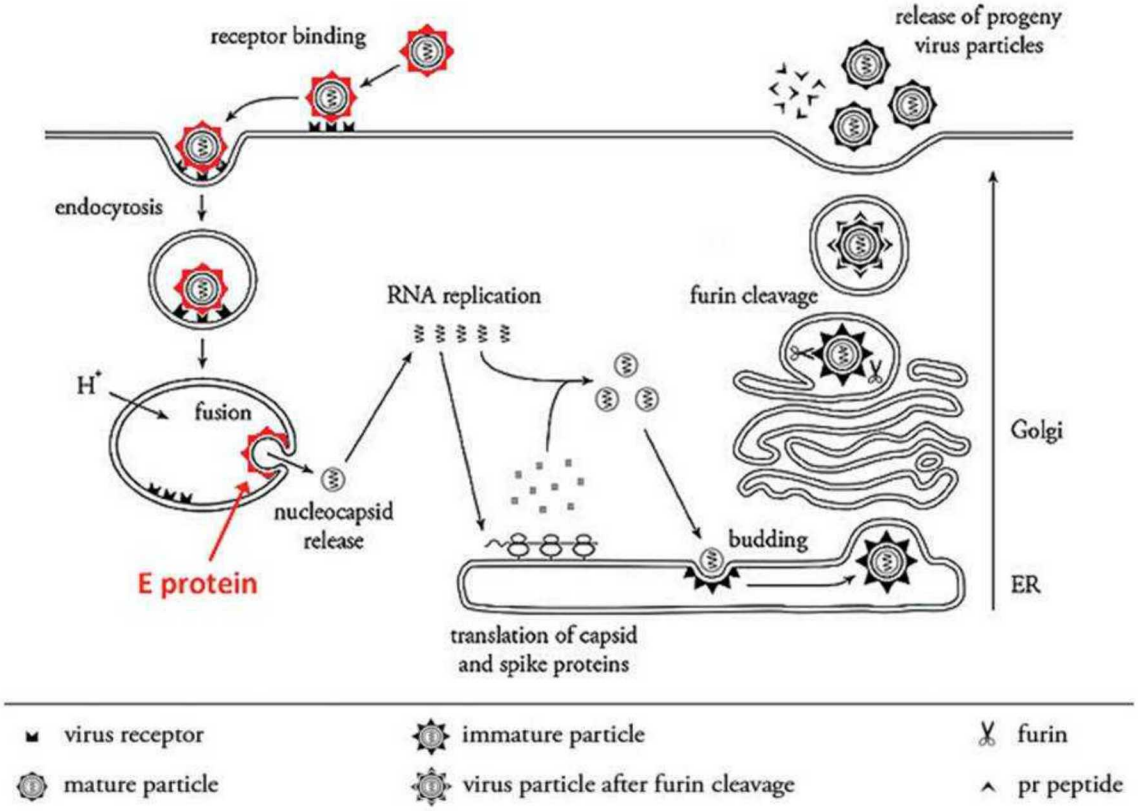

Figure 1.2: DENV life cycle: Cell-receptor-mediated binding initiates virus internalization. Acidification in the late endosome triggers fusogenic E protein trimer formation enabling membrane fusion. RNA replication and viral budding in the ER are followed by furin cleavage in the TGN. Mature infectious virions are released to the extracellular environment via exocytosis. Figure adapted from [2].

Dengue E Fusion

Details regarding the membrane fusion mechanism within the DENV lifecycle are not fully understood, though its characterization has been the focus of many studies [3, 13-15]. The fusion process is of great interest as a therapeutic target, since it is a critical part of the infection pathway. The crystal structure of E has been determined for both the pre- and postfusion states, which has provided important insight into the fusion mechanism; however, speculation remains

concerning the protein conformations and rearrangements that take place from one state to the other.

Prefusion and Postfusion E Protein Crystal Structure

Throughout the virus lifecycle, DENV E exists in one of three conformational states: immature state (before furin cleavage of the pr peptide), mature state, and fusion-activated state [16]. In its mature state, E exists as a dimer that lays tangential to the viral surface at neutral pH, preventing exposure of the fusion loops (FL) of each monomer subunit. The fusion loop is a highly conserved hydrophobic peptide at the tip of domain II that inserts into the host membrane. E is comprised of three distinct domains. These are identified in the linear sequence of the soluble E protein shown in Figure 1.3a for DENV 2. Domain I (DI) is shown in red, DII is shown in yellow, DIII is shown in blue, the fusion loop is shown in green, and the trans-membrane anchor is indicated by blue cross-hatch. When in a non-activated state, the fusion loop is buried beneath DI and DIII, protected from the environment [16]. A ribbon diagram of the atomic crystal structure of soluble E dimer is shown in Figure 1.3b.

The third conformational state exists following low pH exposure. Acidification causes E dimers to dissociate, exposing the fusion loops of each monomer. These fusion loops associate with the lipid membrane and collect to form trimers that have a membrane-insertable hydrophobic "bowl" at the tip; in this state E is considered to be fusion-activated [8]. Domain III rotates around domain I and binds to its side. The stem region, a flexible strand between domain III and two transmembrane helices anchored into the viral membrane, then zips up along the side of domain II resulting in the conformation of the post-fusion trimer. A ribbon diagram of the atomic crystal structure of soluble E trimer in the post-fusion conformation is shown in Figure 1.3c.

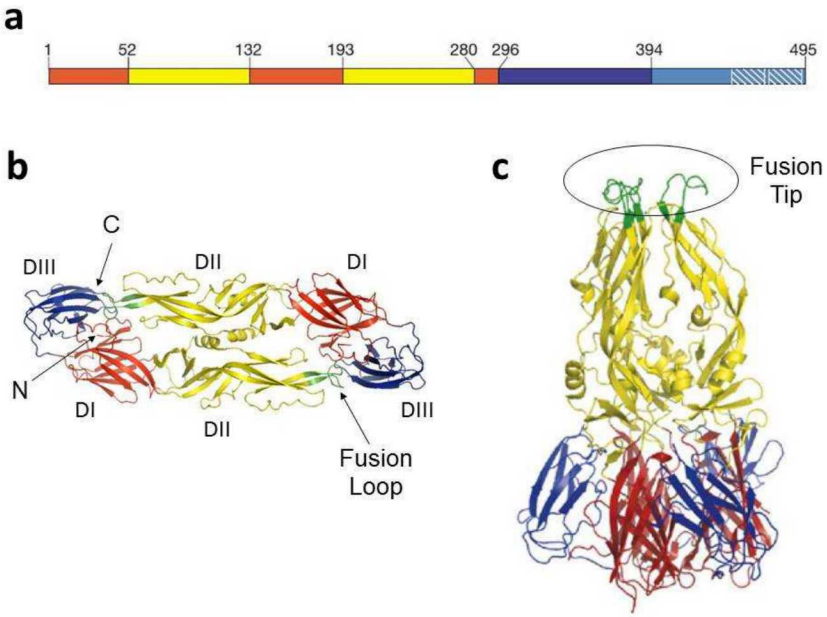

Figure 1.3: Soluble E protein structure: (a) 495 residue sequence of E monomer with DI in red, DII in yellow, DIII in blue, and trans-membrane region in blue cross-hatch. (b) Ribbon structure of prefusion E dimer. Domains I, II, and III are indicated, with DI located at the N terminus and the fusion loop located at the C terminus. Figures (a) and (b) adapted from [8]. (c) Ribbon structure of postfusion E trimer. Fusion loops from E monomers cluster to form a hydrophobic fusion tip. Figure (c) adapted from [16].

Hypothesized Fusion Mechanism

Understanding the prefusion and postfusion states of the E trimer has led to hypotheses regarding the intermediate states and conformational rearrangements that take place during fusion. Figure 1.4 depicts a hypothesized transition between the prefusion and the postfusion conformations leading to fusion. In Frame 1, the drop in pH causes E homodimers coating the viral surface to dissociate into monomers, which are shown anchored to the viral membrane (white) and able to insert the fusion loop into the target membrane (red) and form trimers. DIII begins to fold back against the DI/DII core, moving closer to the fusion loop. The stem region of the protein follows the rearrangement of DIII and begins to zip up along DII, as shown in Frame 3. Though it is not known how many trimers are needed to facilitate fusion, membrane alteration upon E insertion and the free energy associated with conformational changes of E are thought to be sufficient to make membrane fusion energetically favorable [18, 30-32]. Negative curvature develops around the inserted fusion loop, and the outer leaflets of the two membranes merge (hemifusion) forming a stalk as DIII folds back against DI and DII and the stem begins to zip up along DII (Frame 3). As association of the stem and DII is completed, the stalk opens to a pore which expands and the contents within the viral capsid are released into the cytoplasm of the infected host cell (full fusion). Frame 4 depicts the final postfusion state of the E trimer, where the fusion loops and the transmembrane domains are now colocated [5, 14].

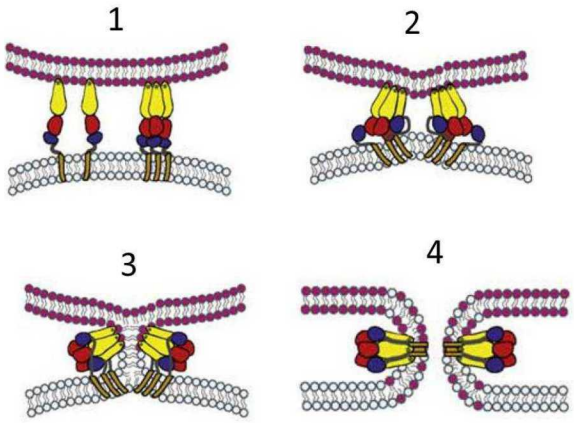

Figure 1.4: Proposed mechanism for membrane fusion: (1) Monomer fusion loop inserted into the target membrane (red). (2) Monomer clustering in the membrane forms fusogenic trimers and negative curvature begins to develop around the fusion loop. (3) DIII folds back towards the fusion loop and the stem region begins to pack against DII, resulting in hemifusion. (4) The stem associates with DII along the full length, achieving fusion and creation of a membrane pore; trimers are in the final postfusion state. Figure adapted from [5].

Another illustration of pre-fusion dimer, post-fusion trimer, and a proposed intermediate structure of E is shown in Fig 1.5. In the pre-fusion and post-fusion states, the fusion loop (FL) is buried in a membrane, and so the FL is only exposed over a timescale of only 5-10 minutes during which it must insert into the endosomal membrane. If the virus does not bind to the endosomal membrane during this time the energy supplied by the conformational change will be lost and the FL will become buried in the viral membrane, and fusion will not occur. The

number of trimers involved, the amount of membrane bending, and the conformation of the trimers upon contact with the host membrane are all important unknown factors. Other factors that may be critical to the fusion process include the affinity of the virus particle for the endosomal membrane as a function of pH, the anchoring energy (the energy required to remove the tip of E from the membrane after it has inserted), the energy required to distort or bend the endosomal and/or viral membrane to the extent needed for fusion to occur, and structure or conditions or interactions that promote merging of the outer leaflets of the two membranes such as fluctuations in the structure of the lipids (i.e. splaying of the lipid tails).

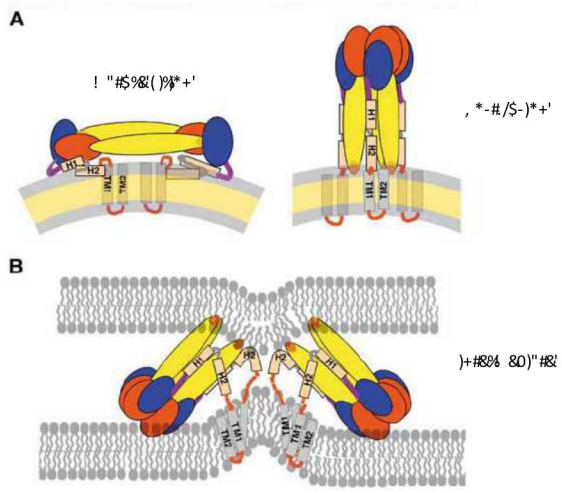

Figure 1.5: Proposed structures for E in association with viral and host membranes. (A) prefusion dimer and post-fusion trimer in association with the viral membrane. (B) Proposed intermediate structure of E upon exposure to low pH in the endosome. The fusion loop is exposed over a timescale of several minutes during which it must insert into the endosomal membrane. Figure adapted from [??].

Regarding the interaction of E with the endosomal membrane we will show that the interaction is not reversible and so we distinguish between the initial affinity of the VLP for the endosomal membrane (energy that determines the extent of VLP binding to the membrane as a function of VLP concentration) and the anchoring energy (energy required to pull the protein out of the membrane after it has inserted). These are illustrated in Figure 1.6. The illustration depicts the binding, insertion, and unbinding of trimers of the free soluble form of E (sE) to a lipid membrane. Both the free soluble form of E and VLPs were used in the experiments reported below, and the concepts illustrated in Figure 1.6 are relevant for either case. We also note that it is unclear whether free sE interacts with membranes as a monomer or a trimer. A conceptual free energy diagram is also shown. The interactions that control the initial extent of binding (the affinity of E for the membrane) lead to a small decrease in free energy upon binding. These interactions occur on a fast time scale and are reversible. However, upon binding the tip of E inserts, lipids rearrange around the inserted tip and the structure of sE may conform to the lipid environment to generate an induced fit, lowering the free energy further. In addition, if sE initially binds in the monomeric state, then trimerization will occur upon insertion, further lowering the free energy. To remove E from the membrane after insertion therefore requires greater free energy than that which governs the binding interaction. Depending on the timescale,

experiments that probe binding may measure the transition from state 1 to state 2, but could also measure a part of the transition from state 2 to state 3. In this work we have developed methods to study the binding affinity (transition from state 1 to either state 2 or state 3) as well as unbinding energy or anchoring energy (the activation energy in the transition from state 3 to state 4). The binding affinity was probed using a quartz crystal microbalance (QCM), whereas the anchoring energy was measured using coflotation of membrane bound protein with liposomes and subsequent centrifugation. Both approaches will be described in detail below.

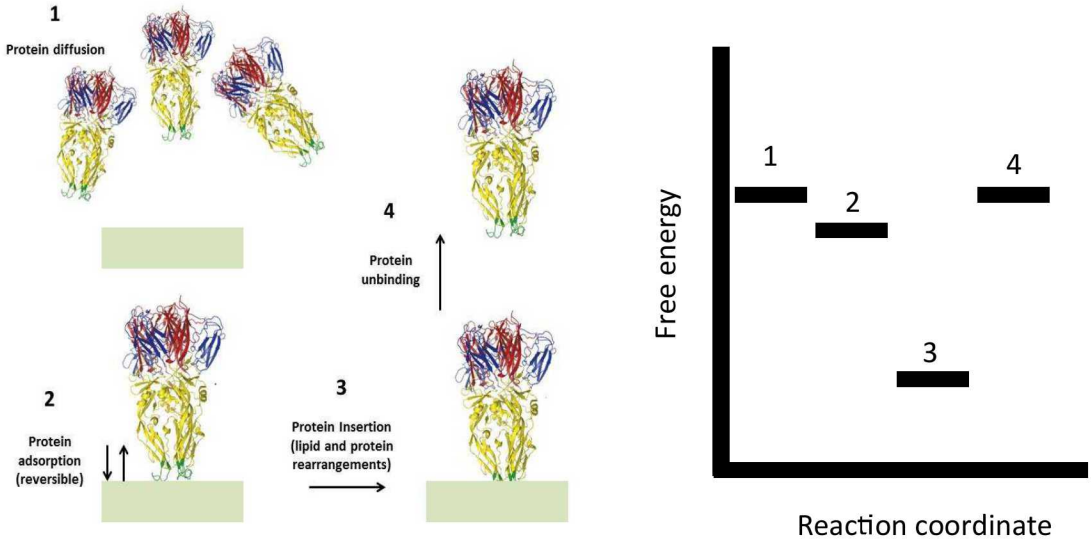

Figure 1.6: Illustration of the binding, insertion, and unbinding of E trimers with lipid membranes along with a conceptual free energy diagram.

Importance of membrane composition

One important consideration regarding the fusion mechanism of DENV is the importance of specific lipids in the target membrane to the fusion process. Specifically, insight into how membrane composition and charge affect E protein binding, anchoring, trimerization, the free energy for initiation of a fusion stalk, and pore formation will provide important information. Regarding membrane composition, recently it was reported that full fusion to target membranes (plasma, endosomal, liposomal) only occurs with membranes containing anionic lipids (AL).[1] The plasma membrane of mammalian cells are rich in cholesterol but lack AL. Early endosomes resemble plasma membranes but endosomes become enriched in AL over time. The discovery that AL are required for fusion means that fusion in mammalian cells occurs only in late endosomes, while fusion does not occur at the plasma membrane or in early endosomes. While the reason for this strong dependence on AL is currently unknown, it was hypothesized that AL facilitate the transition from the hemifusion stalk to pore formation and full fusion. In particular, it was hypothesized that AL facilitate insertion of the fusion loop and trimerization of E. The authors suggested that absent AL, trimerization of E either does not happen or else happens very

slowly. Regarding cholesterol, different conclusions have been reported. One group reported that cholesterol is not absolutely required but increases the efficiency of hemifusion (lipid mixing assay) for the flavivirus tick-borne encephalitis (TBE) with liposomes.[2] Conversely another group reported that addition of cholesterol effectively blocks fusion of DEN in mammalian cells.[3] Others reported that fusion of DENV to the plasma membrane of insect cells was independent of cholesterol.[4] The plasma membrane of insect cells has a high concentration of AL. In that regard, another group reported that in the presence of AL, cholesterol has no effect.[1] Much of the confusion is likely due to the fact that in some cases the effect of cholesterol was examined in the presence of anionic lipids, whereas in other cases AL were absent. Further investigation of membrane charge and cholesterol dependence may provide answers to key questions regarding the fusion mechanism. We note that the envelope protein of alphaviruses has been shown to have a specific interaction with cholesterol,[4,5] whereas no such specific lipid interaction has been found for E of flaviviruses.

Much of the work described below compares binding (free E and VLPs) and fusion for membrane compositions similar to those of plasma membrane/early endosomes (no AL, 30% cholesterol) and late endosomes (30% AL). We will refer to the former as PM and the latter as LE.

Importance of the fusion loop

Another important consideration is the role of the FL to the fusion process. A great deal of evidence indicates that the sequence of the FL of DV is crucial for fusion. This suggests that the positioning and interactions of the fusion loop within the bilayer may be crucial. Certain residues of the amino acid (AA) sequence of the FL are highly conserved. W101, F108, and K110 are conserved among 33 different flaviviruses.[6] Mutational studies have shown that amino acids with either a small side chain or without a side chain are critical at positions 102 and 104.[7] The crystal structure indicates that at position 106, a hydrogen bond occurs between the main chain carboxyl oxygen of G106 and the indoleamine of the W101 side chain. It has been suggested that this H-bond permits W101 to penetrate into the hydrocarbon layer. AA substitutions at position 106 that do not allow for the correct H-bond with W101 adversely affect fusion. Mutational studies also showed that W101 cannot be replaced with other hydrophobic or aromatic AAs, implying that fusion requires precise positioning and orientation of W101 within the membrane. Trp residues have a strong tendency to position within the membrane such that the aromatic ring is aligned with the lipid hydrocarbon tails and the polar portion is oriented toward the headgroups. Based on the crystal structure of the E post-fusion trimer, it was suggested that W101, L107, and F108 form a hydrophobic rim of a concave bowl that anchors the E trimer into the hydrocarbon tails.[8] Single, double, and triple deletion mutants at these three positions resulted in noninfectious virus.[7] Confocal imaging indicated that internalized particles were trapped within endosomes, demonstrating that all three residues are required for fusion. Based on the hypothesis that these hydrophobic residues insert into the hydrocarbon layer while carbonyls and charged residues limit penetration, it was hypothesized that the E trimers penetrate about 6 Å into the endosomal membrane.[7,8] It appears that the bowl cannot accommodate lipid headgroups, so its formation would result in a substantial disruption of the lipid layer. This suggests that the FL-clustered form of the E trimer may not form upon insertion but more likely forms upon zipping up of the stem region along the seam between adjacent domains II of the

trimer.[9] Finally, we note that several fusion-impairing mutations also decreased binding to Mabs 6B6C-1 and 4G2, indicating an altered conformation of the A1 epitope.[7]

While the above evidence strongly suggests that the sequence, structure, and membrane positioning of the FP are critical for fusion, the basis for the extreme sensitivity to these aspects is not yet clear. Some have suggested that the FP serves to anchor E into the host endosomal membrane. However, it has been shown that negatively-charged lipids in the endosomal membrane are essential for full fusion to occur and in that case anchoring is dominated by electrostatic interactions.[10] This strongly suggests that the FP serves a critical role other than anchoring. In that regard other work suggests that the fusion peptide in influenza also plays a critical role other than anchoring, facilitating initiation of membrane fusion by promoting splaying of protrusion of one tail into the polar layer past its phosphorus atom.[11,12]

Overall Aim and Accomplishments of This Work

The goal of this work is to further elucidate the mechanism of membrane fusion that enables DENV infection and virus propagation. This knowledge will also be useful for understanding the fusion process of other important enveloped virus pathogens that utilize similar fusion proteins and mechanisms for infection. The specific aim of this work is to examine the biophysical phenomena governing the roles of the target membrane composition and the FL in DENV fusion.

In this study the following hypotheses were examined: 1) E inserts to the same depth for membranes containing AL or cholesterol; 2) five trimers per VLP or virus interact with the endosomal membrane; 3) strong affinity requires AL (cholesterol alone is not sufficient); 4) strong anchoring requires AL (cholesterol alone is not sufficient); 5) fusion (lipid mixing) occurs only with AL (cholesterol alone is not sufficient); 6) trimerization of E either does not occur or occurs very slowly in membranes lacking AL (cholesterol alone is not sufficient); 7) the FP plays a critical role in the fusion process beyond simply anchoring E into the host membrane. To develop the ability to test these hypotheses we have developed entirely novel methods to i) measure the structure of E in association with lipid membranes, ii) model the interaction of E with lipid membranes, iii) measure the strength and kinetics of the binding of E and VLPs with lipid membranes, and iv) measure the anchoring (pull-out) energy of E imbedded in lipid membranes.

The devastating effects of DENV serve as motivation to characterize the infection pathway of the virus with the aim to develop antiviral therapies that inhibit key steps of the infection pathway. No therapies currently exist to treat DENV, and further understanding of the viral fusion mechanism may reveal potential targets for inhibition. Potential targets for blocking the fusion process include inhibiting trimer formation, blocking the rotation of domain III around domain I, blocking the association of the stem region with domain II to inhibit the zipping up process, and decreasing the strength of the interaction of the E with the host membrane (either the initial affinity or the anchoring energy). Knowledge of the function of lipid composition and the fusion loop in the fusion process will lead to important insights regarding the overall fusion mechanism, and may lead to the development of new therapeutic approaches. In that regard we note that a particular challenge for developing fusion inhibitors for flaviviruses (and alpha viruses) is that many potential targets such as the fusion loop are exposed only for a brief time and only inside the endosome. Therefore either sufficient free drug must get into the endosome

along with the virus, which is highly unlikely, or the drug must bind to E in the mature form of the virus outside the endosome (E in dimer form) and block fusion inside the endosome.

2. EXPRESSION OF E AND PRODUCTION OF VLPs

2.1. Expression of wild type and mutant E

To facilitate experiments investigating DENV fusion with isolated E protein alone, we produced recombinant Dengue serotype 2 E protein derived from the New Guinea C strain sequence. On the advice of our collaborator Dr. Margaret Kielian, we produced the protein in drosophila S2 cells. The expression construct plasmid (pMT-BiP-V5-HisA/D2 sE'-ST or STST) and S2 cell lines transformed with the wild-type sequence encoding the protein's soluble portion were a kind gift of Dr. Kielian. These expression constructs additionally contained either one or two Strep-Tag™ (IBA Biotagnology) epitope tag sequences to facilitate purification. Initial efforts to purify the singly strep-tagged protein resulted in very low (<200ug/L of culture) yields, while subsequent use of the double strep-tag version gave far better results (600-800ug/L of culture).

S2 cells were grown in SFX-Insect medium (Thermo Hyclone). Initially, we used alternative serum-free media (Insectagro-DS2, Life Technologies) but obtained mediocre growth rates relative to other media and poor protein yield. Shaking cultures in 2L baffled flasks containing 600ml of medium were inoculated at 3-6 x 10^6 cells per ml and copper sulfate was added at a final concentration of 1mM on culture day 0. On day 7-9, culture supernatant was harvested by centrifugation at 13,000 x g, 15min, 4°C. For each batch, a total of 8L of clarified and 0.2um-filtered supernatant was then concentrated to 1L using Vivaflow 200 concentrators (Sartorius, 10,000 KDa cutoff). Egg white avidin (Life Technologies) was then added to the supernatant at a final concentration of 15ug/ml to bind free biotin that would interfere with purification, and the pH was slowly adjusted to 8.0 using 0.5M NaOH with rapid stirring. During our efforts, we determined that buffer exchange was unnecessary for binding to streptactin and generally caused formation of a crystalline precipitate that clogged the affinity columns. Supernatant was then passed over two 1ml streptactin columns (Qiagen) in series at a flow rate of 1ml/min. GE Healthcare branded streptactin columns performed poorly relative to the Qiagen. Columns were washed with 40ml PBS pH8 then eluted using 5mM desthiobiotin (Sigma) in wash buffer. Buffer exchange (1:100-1:500) and concentration were done using centrifugal ultrafiltration and TAN buffer (20 mM triethanolamine, pH 8.0, 130 mM NaCl). Purified protein in TAN buffer was quantified by UV spectrophotometer (NanoDrop2000) using a calculated MW of 46,906 Da and ε of 59,190. Aliquots were stored at -80°C.

Mutants of the E protein expression construct (W101F, F108A, W101F/F108A) were generated using standard site-directed mutagenesis (QuickChange II, Agilent) and confirmed by Sanger sequencing. Our goal was to produce these mutant recombinant E proteins in order to evaluate the functional contributions of these residues in binding, fusion, and monomer/dimer/trimer formation. The verified mutant plasmids were linearized and transfected into S2 cells either by Nucleofection (Lonza) or cationic lipids (XtremeGene HP, Roche). Despite four separate attempts, we were unable to recover viable clones from the transfected pools. It is worth noting that the expression plasmid as sold by Life Technologies contains the blasticidin resistance gene, but the line we received from Dr. Kielian is puromycin-resistant, suggesting either the original plasmid they used was modified or that a puromycin resistance plasmid was co-transfected when they made that S2 line. If this effort resumes, it is possible switching to puromycin resistance may give better results.

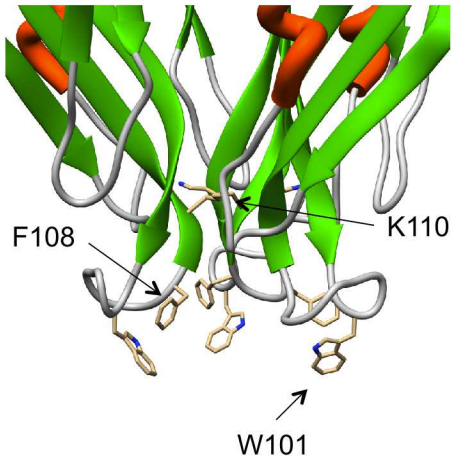

Figure 2.1: Illustration of the location of the mutations introduced into the fusion loop of E (tip of domain II) in this work.

2.2. Expression of wild type and mutant VLPs

In order to investigate DENV fusion kinetics, inhibition, and lipid/cholesterol dependence using classical fusion assays, we produced virus-like particles based on sequence from the DENV1 Western Pacific strain virus. The tetracycline-inducible stable 293-based cell line was a gift from Dr. Margaret Kielian. This line was made by stably transfecting 293-Trex cells (Life Technologies) with a plasmid containing the DENV1 wild-type prME sequence and Tet operator.

The 293-Trex/DV1-VLP cell line was grown in DMEM-10% FBS medium with 10ug/ml blasticidin and 200ug/ml zeocin on 15cm tissue culture-treated plates. When cells were 75-90% confluent, tetracycline was added at a final concentration of 1ug/ml and cultures were incubated for 48hrs before harvesting supernatant. To purify and concentrate VLP, 40% PEG 8000 in PBS was added to culture supernatant at a final concentration of 8%. This mixture was incubated overnight at 4°C then centrifuged at 10,000 x g for 30min. The PEG-precipitated pellet was then layered on top of an Optiprep (in PBS) gradient with range 40-5% in 5% increments and centrifuged at 35,000 x g for 2hrs. The VLP fraction (25%) was then removed using a syringe and needle then buffer-exchanged with TBS using a 100kDa centrifugal ultrafilter. Aliquots were stored at -80°C.

In order to facilitate both labeling and functional studies, we produced mutant VLPs. The pCDNA3/TO-DV1 prME plasmid was modified using QuickChange II site-directed mutagenesis (Ambion). The mutants produced were (relative to full-length wild-type sequence): W101F, F108A, K110E, and W101F/F108A. The three functional mutants plasmids were transfected into 293-Trex cells by Nucleofection (Lonza, Kit V). Clones were isolated by limiting dilution and screened for expression of DV1 E protein (by immunoblot) then VLPs were produced as described above. The mutants produced for labeling were also transfected into 293-Trex cells,

but were frozen as polyclonal pools due to lack of time. If future efforts require VLPs bearing these mutations, the frozen polyclonal pools should be cloned prior to VLP production.

3. STRUCTURAL STUDIES OF E BOUND TO PC:PG AND PC:PE:CH BILAYERS

3.1 Neutron reflectivity studies of structure of membrane-bound E

NR is one of very few methods that can resolve structural details of membrane-associated proteins in physiological conditions, and may be unique in its ability to directly resolve details of the full membrane-bound protein structure, in contrast to techniques that probe only labeled residues or secondary structural elements. NR involves measuring the ratio of reflected to incident intensity as a function of momentum transfer $q_z = 4\pi sin\theta/\lambda$, where q_z is the angle of incidence with respect to the plane of the membrane and λ is the wavelength.[13] The form of this curve is determined by the in-plane averaged scattering length density (SLD) profile normal to the surface. The SLD is directly related to the atomic composition and the density. Therefore, for a protein bound to a planar lipid membrane, NR determines the in-plane averaged distribution of amino acid residues normal to the membrane, and is sensitive to any changes in that distribution.

Several platforms are used to study conformational changes of proteins interacting with lipid membranes by these methods. Each has advantages and limitations, and the information from different platforms must sometimes be combined to obtain the most complete picture. The Langmuir monolayer is a platform that is simple to implement and for which the data analysis is straightforward due to the fact that only a single lipid layer is present. However, this method requires a relatively large volume of solution (18 ml). This was important in the present study as the protein was available in short supply and was very expensive. Lipid bilayers supported directly on a silicon substrate constitutes a second platform. This has the advantage of requiring much less solution (3 ml) but data analysis and interpretation are substantially complicated by the presence of two lipid layers and the possibility of lipids exchanging between the two layers.

The NR data were analyzed using the Ga_refl program based on the optical matrix method. Ga_refl is available at www.ncnr.nist.gov. Simultaneous fits of the NR data were performed for multiple data sets involving different contrast conditions, and for multiple data sets at different stages of a single adsorption run (for example lipids only, with adsorbed protein, and after subphase exchange). Simultaneous analysis allowed particular characteristics to be maintained constant for all the fits, such as the SLD of the subphase and specific characteristics of the lipid layers. In all cases, the fits included only the minimum number of layers for the protein that were required to achieve a good fit to the data. In the Ga_refl program the roughness parameter is the full width at half maximum (FWHM = 2.35 s, where s is the standard deviation) of a Gaussian distribution and was constrained in the fitting to be less than the smallest thickness of the two adjacent layers.

Fitting reflectivity data results in defining a family of SLD curves that are consistent with the data. The uncertainty in the fitted profiles was determined by a Monte Carlo resampling procedure in which a large number (1000) of statistically independent sets of reflectivity data were created from the original data set and the error bars from the counting statistics. Each set of reflectivity data was analyzed using the fitting procedure described above. The result is a range of values for each fit parameter that is consistent with the statistics of the original data. The fit of

each reflectivity set was initiated with random values for the fit parameters. This method has been reported in detail elsewhere.[14]

3.1.1. Method

Supported lipid bilayers. For the NR measurements tethered lipid bilayers (TLBs) were prepared as described in Heinrich et al Langmuir 25(7), 2009. A cartoon of the tethered bilayer structure is shown in Fig .

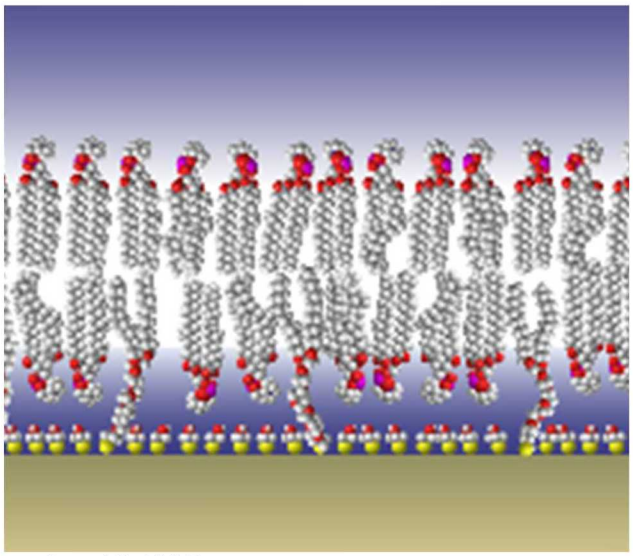

Figure 3.1: Illustration of the tethered lipid bilayer.

After deposition of the TLB, NR data were collected with H_2O buffer and D_2O buffer in the measurement cell. Buffer exchange was accomplished by flushing 10 ml of buffer through the cell (volume ~1.3 ml) using a syringe. The experiments involving Dengue sE were performed using two protocols. In the first, a buffer solution at pH 8 was initially circulated through a small reservoir and the measurement cell containing the tethered bilayer using a peristaltic pump. The protein was added to the reservoir and circulated, and NR data were collected at pH 8. No adsorption was detected under pH 8. The pH was then lowered by adding concentrated MES to the reservoir. The pH meter was monitored with a probe inserted into the reservoir. The pH was lowered in several increments until reaching pH 5.5 and NR curves were collected at each pH increment. At pH 5.5 the circulation system was removed, the solution in the measurement cell was exchanged with H_2O buffer, and NR data were collected. Then the solution in the cell was exchanged D_2O buffer at pD = 5.5 using a syringe. In the second protocol, following collection of NR data for the TLB in H_2O and D_2O buffer, a 2 ml solution of sE in buffer at pH 5.5 was injected into the measurement cell using a syringe. In this case 5% PEG 400 was included to inhibit aggregation of protein and non specific adsorption of protein to the membrane. Short NR scans were collected until adsorption was completed, the cell was exchanged with D_2O buffer, and a full scan was collected. Then the cell was exchanged with H_2O buffer and a full NR scan was collected.

3.1.2. Results

Figure 3.2 shows NR data for a 49:21:30 PC:PE:CH tethered lipid bilayer alone and after sE binding. Figure 3.2 also shows the calculated SLD profile and angular distributions for the best fits. Corresponding data for a 70:30 PC:PG TLB are shown in Figure 3.3. Best fits were determined using a free form slab model, that makes no assumptions about the shape of the SLD profile, and also using the X-ray crystal structure of the sE trimer.

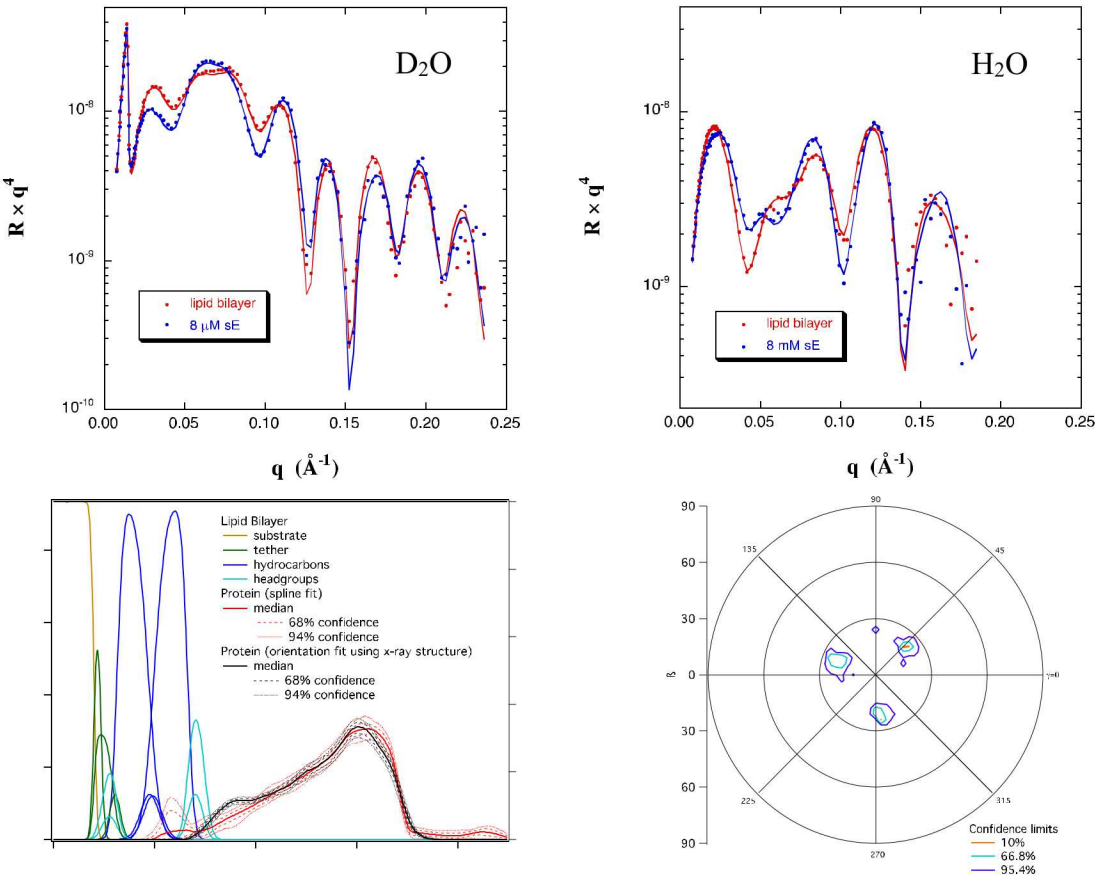

Figure 3.2. NR data for E bound to 49:21:30 PC:PE:CH tethered lipid bilayer. Also shown are calculated SLD profile and angular distributions for the best fits.

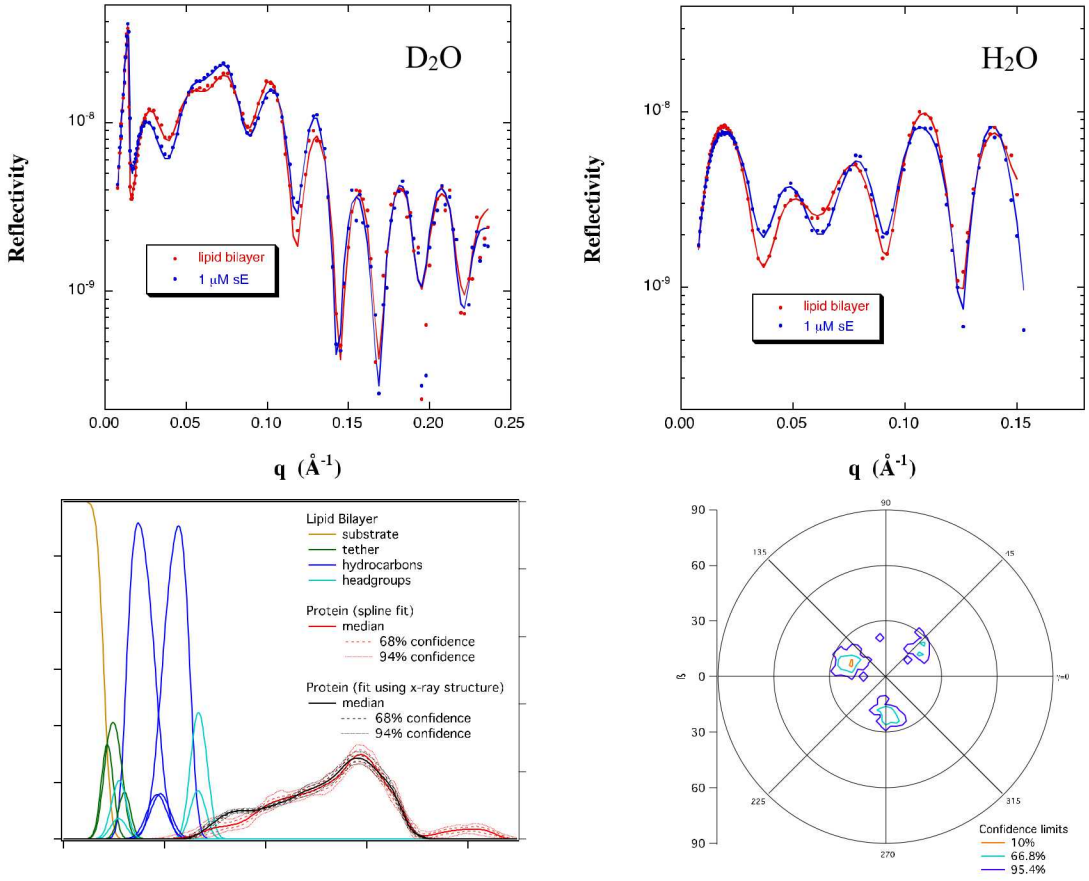

Figure 3.3: NR data for E bound to 70:30 PC:PG tethered lipid bilayer. Also shown are calculated SLD profile and angular distributions for the best fits.

These data show that the final state of the inserted protein is very similar for the two membrane compositions. E is inserted to a depth such that the fusion loop coincides with the interface between the lipid headgroups and the hydrophobic tails. The tip-inserted protein is tilted with respect to the membrane to a similar degree for both membrane compositions.

3.2 Study of membrane curvature induced by insertion of E

In order for fusion to occur the endosomal membrane must bend to join with the viral membrane and form a fusion stalk, as illulstrated in Figure 1.4 and Figure 1.5. In particular the membrane must adopt negative curvature, presumably around the tip of E as it inserts. Therefore it is important to know if the insertion of E naturally induces negative curvature, which would aid the fusion process or positive curvature, which would increase the energy barrier for fusion. To address this, we studied the pressure-area response upon the insertion of sE into Langmuir monolayers of composition 70:30 DPPC:DPPG. It is necessary to use saturated lipids as unsaturated lipids are not stable at the air water interface. In this study the surface pressure was

monitored at fixed surface area as the concentration of sE in the solution was increased by injecting it underneath the lipid monolayer. The results, shown in Figure 3.4 show that immediately after each injection the pressure decreases slightly and then gradually increases. The increase in pressure is substantially larger than the initial decrease. We interpret the initial decrease in pressure as due to decrease in electrostatic repulsion among the lipid headgroups as the positively charged residues of the protein bind to the negatively-charged lipids. We interpret the increase in pressure as due to insertion of the tip of sE into the membrane. These results provide evidence that insertion of the tip of E induces positive curvature in lipid membranes. X-ray reflectivity scans were also performed upon injection of sE. The results at a bulk concentration of 3 μM are shown in Figure 3.5. The results show a shift in the fringe spacing to lower q_z which indicates that the lipid layer becomes thicker. This indicates that the lipid tails, which are tilted slightly in the monolayer prior to injecting sE, stand up straighter upon insertion of sE. This indicates that some residues insert into the lipid tails. The simulations described below show that the tip of E inserts such that the W101 inserts into the lipid tails. This is also consistent with the NR data described above.

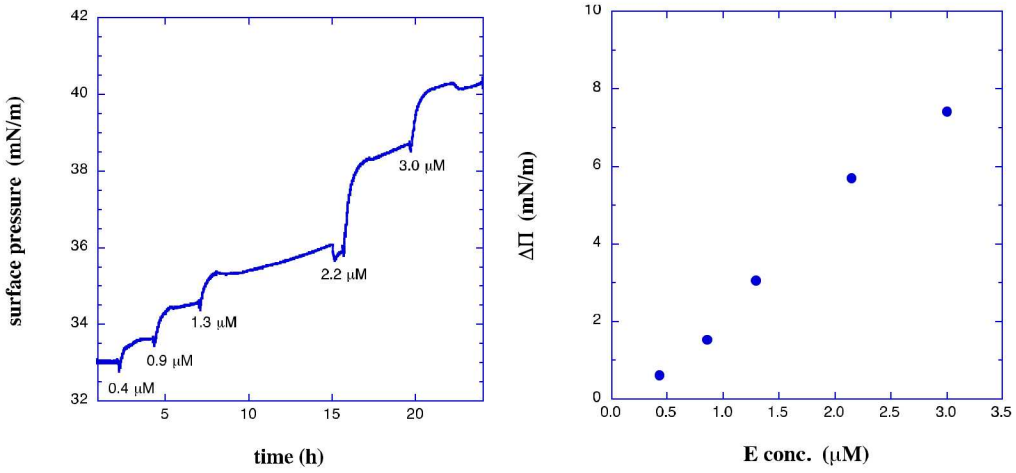

Figure 3.4: Left panel: Surface pressure versus bulk concentration of sE. Right panel: Total increase in pressure versus bulk concentration of sE.

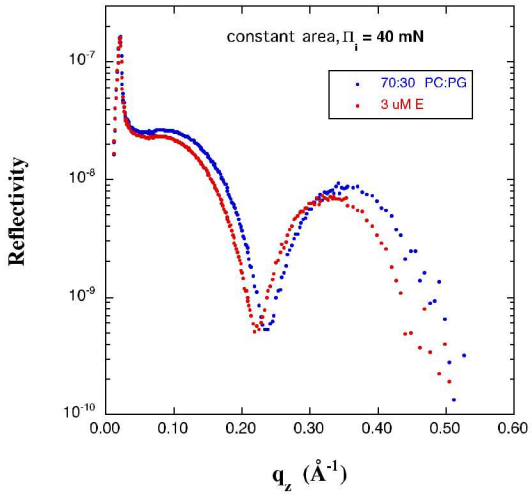

Figure 3.5: X-ray reflectivity for lipid monolayer alone and after increasing the bulk concentration to 3 μM. The shift in the minimum to lower q_z indicates that the lipid layer has slightly increased in thickness.

4. BINDING, UNBINDING, AND FUSION STUDIES

4.1 Dependence of E binding on lipid composition

4.1.1. Method

sE binding studies were acquired using a quartz crystal microbalance with dissipation monitoring (QCM-D). In this method, changes in the frequency (ΔF) and dissipation (ΔD) of an oscillating quartz crystal are used to measure the mass and rigidity of thin films that adsorb to the crystal surface. For a rigid layer, the frequency change is directly proportional to the increase in adsorbed mass by the Sauerbrey equation ($\Delta m = -C\Delta F/n$) where n is the overtone number. A Q-Sense D300 (Biolin Scientific) was used to acquire the data. Quartz crystal sensors were cleaned with detergent, rinsed with copious amounts of water and then dried under N_2. Just prior to the measurement the sensors were placed in a UV-ozone chamber for 30 minutes. Prepared sensors were then loaded into the sample chamber as shown below in Figure 4.1.

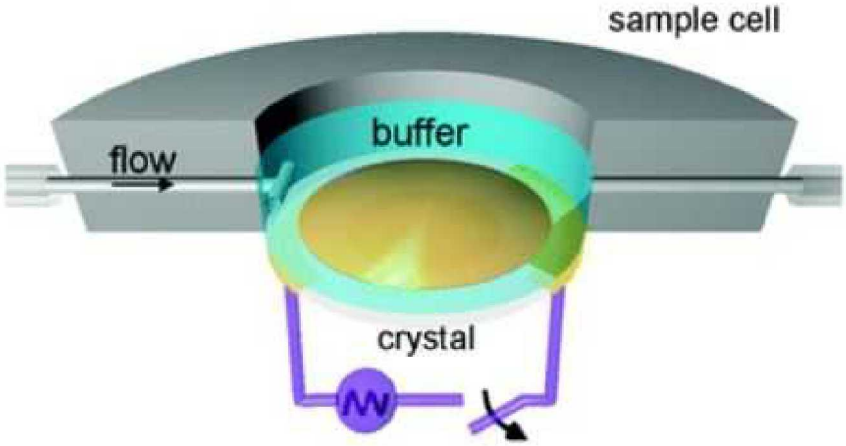

Figure 4.1: Schematic of QCM-D sample chamber: The prepared crystal was placed within the instrument, creating a sealed chamber to hold the liquid sample.

Lipid bilayers were deposited onto the sensors by liposome fusion. A 2 ml solution of 0.1 mg/ml liposomes in buffer was flowed through the chamber. Achieving effective and complete fusion required the use of different buffers for different liposome compositions. For liposomes composed of PC:PG, the buffer composition was 20mM MES, 500mM NaCl, pH 7.0 with 5 mM $CaCl_2$, and for liposomes composed of PC:PE:CH and PC:PE the buffer composition was 20mM MES, 50mM NaCl, pH 7.0 with 5 mM $CaCl_2$. Flow was stopped and the liposomes were allowed to adsorb to the quartz surface for several minutes. For PC:PG liposomes, the liposomes ruptured and fused to the substrate to form a supported lipid bilayer (SLB) within a few minutes. An example of the QCM response is shown in Fig 4.2. The calculated frequency change (normalized by overtone number) for deposition of a complete bilayer is 25-30 Hz depending on lipid composition. The SLB should be fairly rigidly attached to the sensor, so the dissipation

value should return to a value within 0.5 E-6 of the value measured prior to adding liposomes. These values for changes in F and D were used to verify deposition of a completed bilayer and the absence of unfused liposomes. The presence of unfused liposomes is easily detected as a frequency change greater than 25-30 Hz. In the case of PC:PE:CH liposomes, flushing the cell repeatedly with another buffer was sometimes required to cause the liposomes to rupture and fuse to the substrate and form a completed lipid bilayer. After a completed lipid bilayer with absence of unfused liposomes was achieved, as indicated by the frequency and dissipation values, the chamber was then exchanged with buffer at pH 5.5 for studies of sE binding. sE protein solutions were then added to the measurement cell. For each sample, sE was mixed into MES buffer pH 5.5 to the prescribed concentration in either 2ml (used for lower concentration samples) or 1.3ml (used for 3μM and 6 μM samples). 1.3ml is the minimum volume necessary to ensure a complete exchange of the cell volume. After the measurement period, an excess of the buffer solution was flowed through the cell to determine if adsorbed sE bound irreversibly.

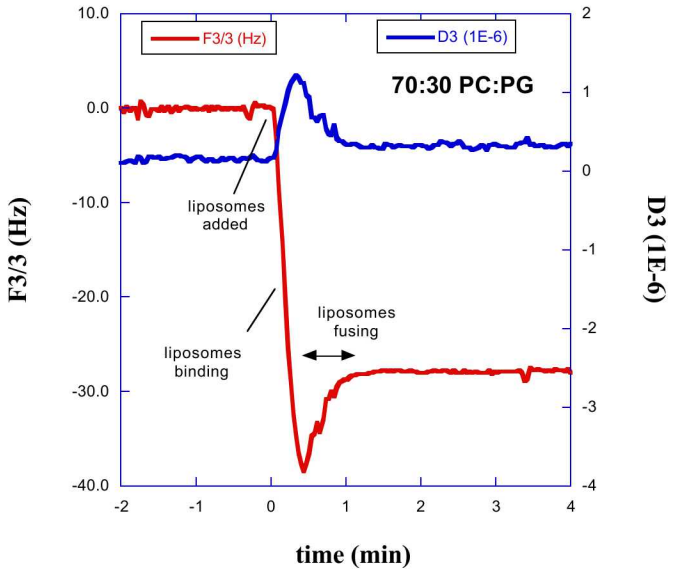

Figure 4.2: QCM frequency (F) shift showing adsorption of liposomes to a QCM sensor followed by rupture and fusion.

4.1.2. Results

Figure 4.3 shows changes in F for sE at 3 μM binding to PC:PG 70:30 lipid bilayers. The three plots compare results for different delay times between injecting sE and flushing the cell with buffer. The results show very rapid adsorption at 3 μM. The results also show that when the measurement cell was flushed 10 min after injecting sE much of the protein was removed by the rinse. However, when the measurement cell was flushed 100 minutes after injecting sE very little of the protein was removed by the rinse. This illustrates the point described in the introduction (see Fig 1.6) that adsorption proceeds initially through a stage of rapid equilibration followed by insertion and induced fit to reach a state in which the sE is bound irreversibly. Analogous results are shown in Figure 4.4 for sE binding to PC:PE:CH 49:21:30 lipid bilayers.

In this case the binding is less rapid and occurs to a lesser extent compared with the data for PC:PG 70:30. Surprisingly, the equilibration stage is apparently much shorter in this case, as sE was entirely irreversibly bound at a delay time of 10 min. Figure 4.5 compares the results for bilayer compositions 70:30 PC:PG with 49:21:33 PC:PE:Chol at 3 μM. The first plot shows the more rapid and stronger adsorption to PC:PG 70:30 liposomes but also the difference in reversibility mentioned above. The second plot compares the fraction removed upon rinsing as a function of the delay time, further demonstrating that the equilibration stage is of longer duration for PC:PG 70:30. The third plot compares the dissipation signals for the two cases. The reversible stage for PC:PG is associated with a greater dissipation than observed for 49:21:33 PC:PE:Chol over the same time period. This is consistent with a more loosely bound adsorbed layer for PC:PG 70:30. The origin of this difference in the timescale of the reversible stage is not understood.

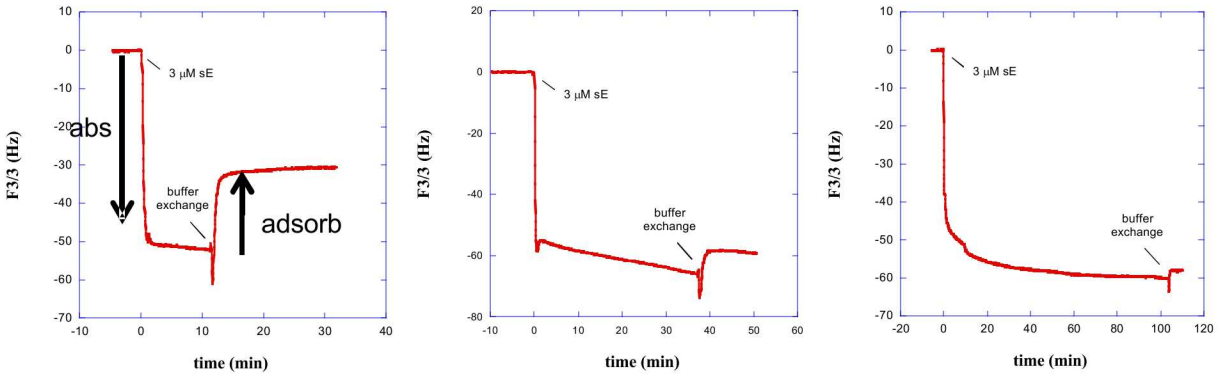

Figure 4.3: QCM frequency changes for sE binding to PC:PG 70:30 lipid bilayers. The binding is partially reversible upon rinsing with buffer after a delay time of 10 min, but is nearly entirely irreversible after a delay time of 100 min.

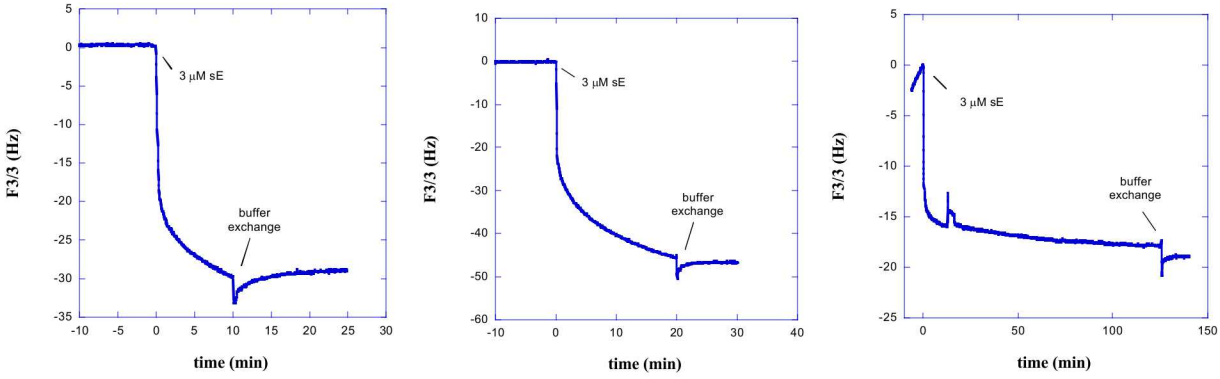

Figure 4.4: QCM frequency changes for sE binding to PC:PE:CH 49:21:30 lipid bilayers. The binding is nearly entirely irreversible after a delay time of only 10 min.

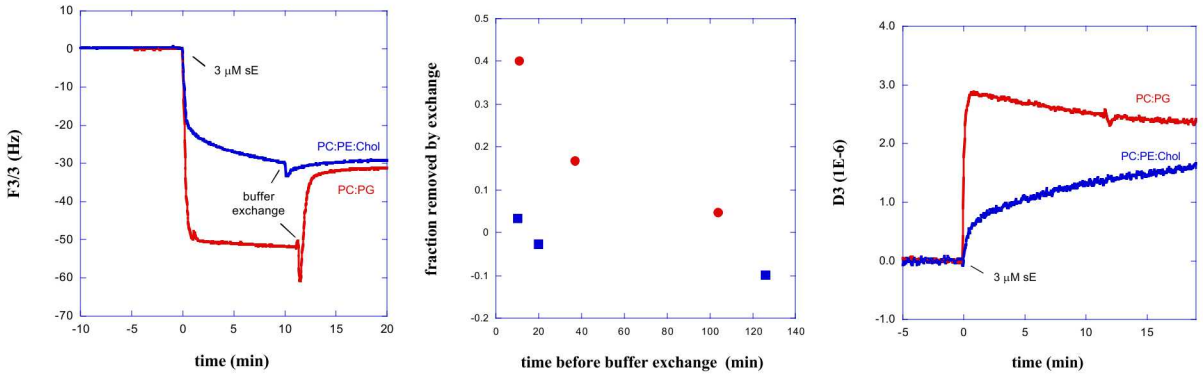

Figure 4.5: Comparing QCM results for bilayer compositions 70:30 PC:PG with 49:21:30 PC:PE:Chol.

Figure 4.6 shows changes in F for sE at 3 μM binding to PC:PE 70:30 lipid bilayers. Very little adsorption occurs compared with the levels of binding for 70:30 PC:PG with 49:21:30 PC:PE:Chol. This demonstrates that in the absence of AL or cholesterol, the binding affinity is very low, and that both AL and cholesterol substantially increase in the binding affinity. Figure 4.7 compares sE binding for membranes with various lipid compositions. The value of the frequency change 30 minutes after injecting sE was plotted in each case. A series is shown involving bilayers with various percent PG. A monotonic increase in binding is observed for the entire range between 10% and 30% PG. At 3 μM, roughly twice as much sE binds to PC:PE 70:30 lipid bilayers as binds to bilayers of 49:21:30 PC:PE:Chol. The binding affinity afforded by 30% cholesterol is slightly less than that provided by 25% PG.

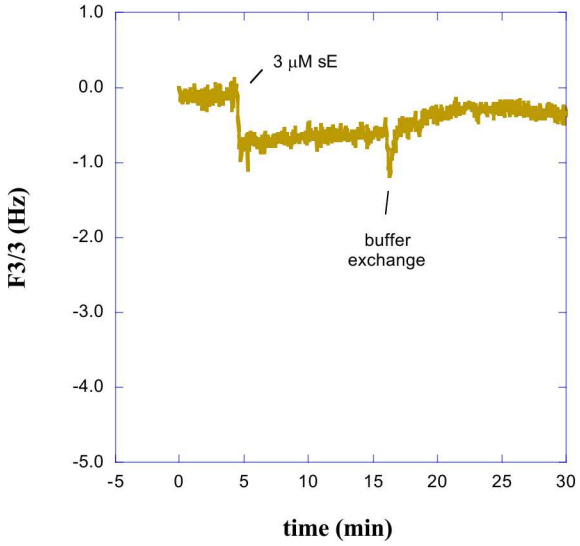

Figure 4.6: QCM frequency changes for bilayer composition 70:30 PC:PE. The adsorption affinity is very low in absence of anionic lipids or cholesterol.

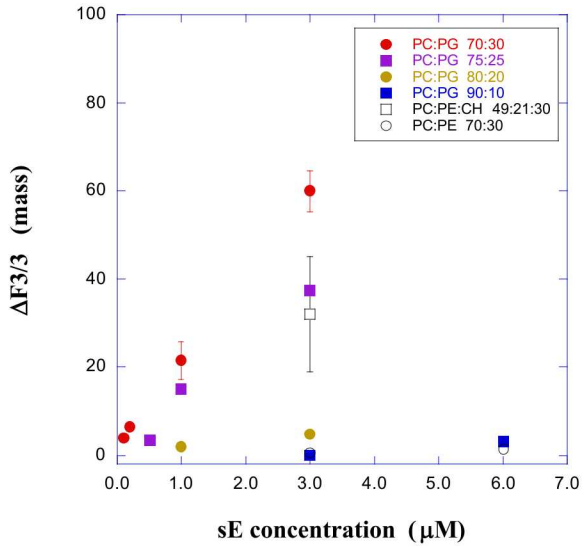

Figure 4.7: Comparison of binding levels for membranes with various lipid compositions. The frequency change 30 min after injecting the solution containing sE is plotted for each lipid bilayer composition.

Finally, we determined that sE forms trimers upon binding to liposomes of composition PC:PG 70:30 and PC:PE:CH 49:21:30. However due to lack of sufficient protein we were unable to determine the rate of trimerization in each case. A difference in the rate of trimerization could explain the difference in timescale of the reversible stage shown in Figure 4.5 although other explanations are possible, such as binding by electrostatic interactions to PC:PG 70:30 in a metastable state such as side-on without tip inserted.

4.2 Dependence of E unbinding on lipid composition

To measure the anchoring energy, or the energy to remove E trimers after they are imbedded in a membrane, we first considered use of atomic force microscopy (AFM). AFM has been used to previously to measure the force required to pull peptides out of membranes.[15] However, there are a number of disadvantages and difficulties with this method. In particular, it is very difficult to attach the AFM tip to only a single protein. In addition, due to limited sensitivity of typical AFMs, the force can only be measured if it is greater than 10 pN. So it is appropriate to pullout transmembrane helices, but proteins that are more weakly inserted will be difficult or impossible to measure by this method. In addition, converting the force to an energy also involves difficulties in that the force depends upon the rate of retraction of the cantilever.[16] In this work we discovered and developed an entirely new biophysical method to measure the anchoring energy of membrane inserted or membrane-associated proteins. The method is based on coflotation of proteins bound to liposomes in a sucrose gradient, wherein unbinding is followed as a function of time and temperature upon spinning in an ultracentrifuge.

4.2.1. Method

Liposome coflotation is a technique commonly used to assay for binding of proteins to lipid membranes. We determined that a slightly altered methodology could be used to determine the energy required to remove proteins from membranes after they are bound (anchoring energy). The methodology of liposome coflotation used to probe E protein anchoring into liposomes is as follows (see Figure 4.8): unilamellar vesicles were combined with E protein and the reaction mixture was acidified. E protein interacts with the liposomes at low pH and binds to the lipid membranes. The reaction mixture was then deposited in a sucrose gradient, and upon centrifugation, membrane-bound and unbound E protein moved to different locations within the gradient according to the respective densities. Liposomes, and any associated protein migrated to the top of the gradient since the density of liposomes is lower than that of the sucrose layers. Unbound protein migrated to the bottom of the gradient since the density of protein is higher than that of the sucrose gradient. After a short spin, the liposomes reach the top of the gradient along with any attached protein. However, we discovered that after more extended spinning times, the bound protein will detach from the liposomes and migrate to the bottom. Assuming the detachment is a first order rate process, by measuring the rate of detachment as a function of time for different temperatures the activation energy for detachment can be determined using the Arrhenious equation (Figure 4.9). The fraction of E protein that remained bound to lipid membranes after spinning for various was determined using western blots.

The time required for liposomes to reach the top of the gradient at the maximum speed of 54000 rpm was about 30 min, determined by using fluorescent dye as shown in Figure 4.10.

To achieve a high level of binding while at the same time using a low amount of protein, the E protein and liposomes were incubated together for 4 hrs at pH 3 and 20 C.

Sucrose gradients were made in Beckman Ultra-Clear 5mm x 41mm centrifuge tubes in a total volume of 700µl. The volume for each layer was scaled down in relation to previous protocols that utilize larger volume tubes [3, 14]. Figure 4.8 shows a schematic of the gradient layers, along with the corresponding volumes and sample placement before centrifugation. Liposome-protein samples were adjusted to a 20% sucrose solution at a final volume of 133µl and applied to 100µl of a 40% sucrose cushion. The sample was overlaid with 400µl of a 15% sucrose solution followed by 67µl of a 5% sucrose solution. The pH of each sample was maintained within the gradient by using sucrose solutions made in TAN buffer, pH 8.0 or in MES buffer (50mM MES, 100mM NaCl), pH 5.5. Gradients were subject to centrifugation for times ranging from 1 hr to 65 hr at speeds ranging from 27,000rpm to 54,000rpm at temperatures ranging from 20 ˚C to 40 ˚C using a Beckman SW55Ti rotor [3, 14, 17]. 250µl fractions were then collected from the gradient by hand using a glass syringe. A total of 5 fractions were collected. The relative amount of protein in each fraction was determined by western blot using the 4G2 antibody. A sample western blot is shown in Figure 4.11. The strongest band was normalized to unity, and the intensities of the bands for the other fractions were determined relative to the strongest band. The band intensity for the top fraction divided by the sum of the band intensities for all five fractions was reported as the fraction of bound protein.

We note that this method is suitable only for a limited range of anchoring energies. The higher limit is determined by the slow rate of unbinding at the lowest temperature used. In this work the lowest temperature used was 20 ˚C and a spin time of 65 hrs was required to measure unbinding for liposomes of composition PC:PG 80:20. Greater anchoring energies could be measured by using higher temperatures during spinning. However, the ultracentrifuge used in

this work is rated to a maximum temperature of 40 ˚C. The lower limit of anchoring energy is determined by the fast rate of unbinding at the highest temperature used. In particular the limit is reached when the rate of unbinding approaches the time required for liposomes to migrate to the top of the gradient. In addition, a low anchoring energy likely corresponds to a very low affinity of the protein for the membrane, and therefore a very high protein concentration is required to achieve a sufficiently high level of binding as needed for this method.

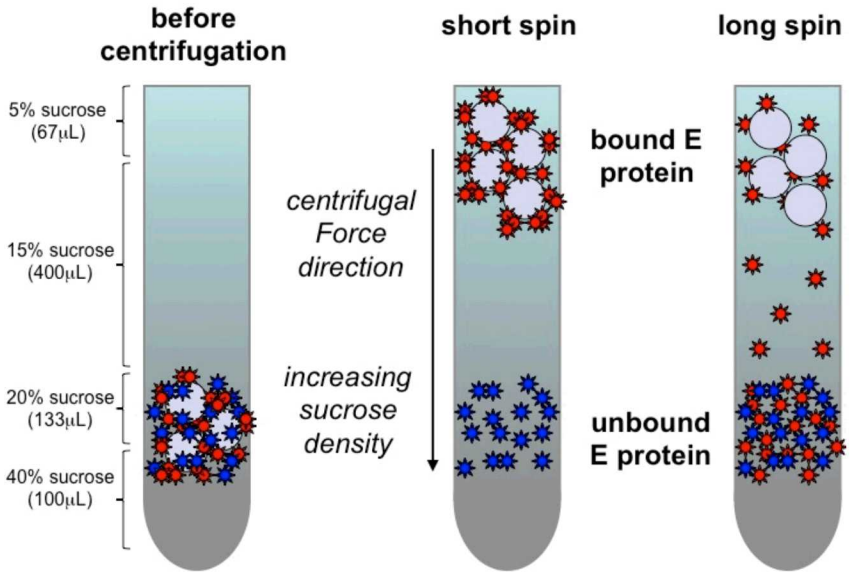

Figure 4.8: Illustration of the method used to determine the energy to remove E from a lipid membrane. The grey circles represent liposomes.

$A \rightarrow P$ first $\frac{d[A]}{dt} = -k\,[A]$ $\ln[A] = \ln[A]_0 - kt$

First order integrated rate law: $\ln[A] = \ln[A]_0 - kt$

A plot of ln[A] vs *t* will be linear with a slope of *-k*.

The Arrhenius equation: $k = Ae^{-Ea/RT}$

Figure 4.9: First order rate analysis used to determine the energy to remove E from a lipid membrane.

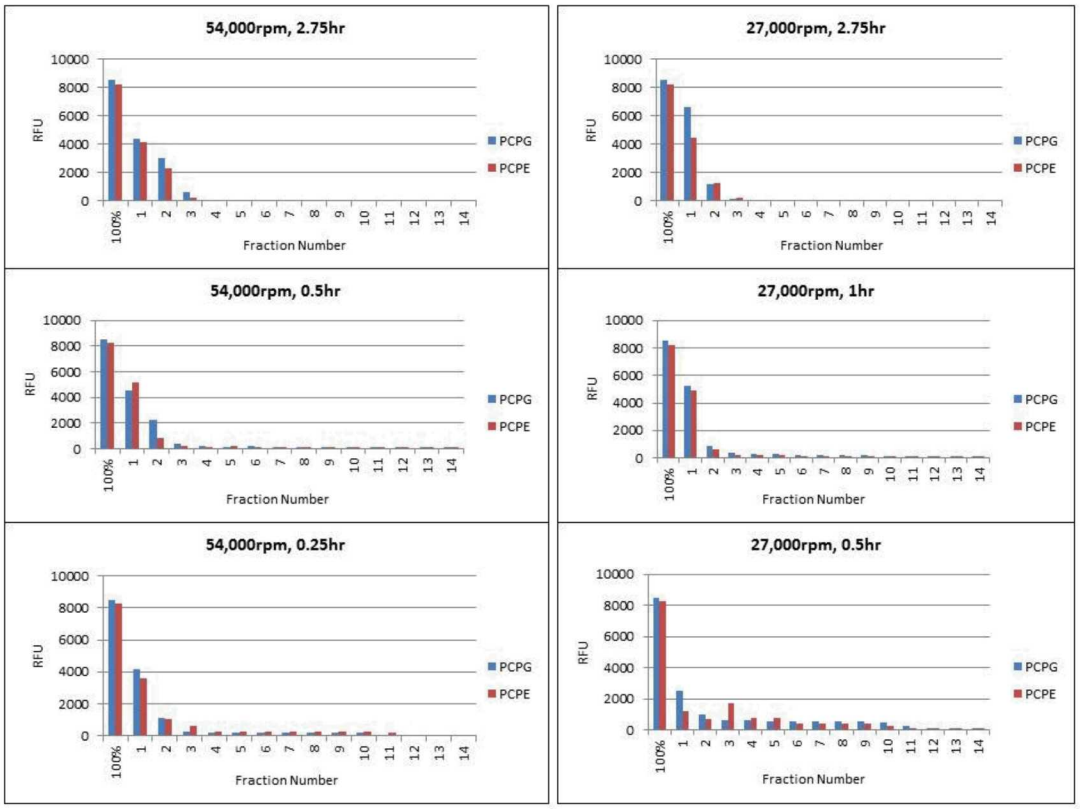

Figure 4.10: Liposome fluorescence measurements: Fluorescent liposomes demonstrate where vesicles migrate within the sucrose gradient for given centrifugation conditions. 70:30 PC:PE and PC:PG with 3%Dansyl-PE were examined at 54,000rpm and 27,000rpm, and time points ranged from 0.25hr to 2.75hr. Centrifugation at 54,000rpm and 27,000rpm required a minimum time of ~0.5hr and ~1hr, respectively, for lipsoomes to fully migrate to the top of the gradient.

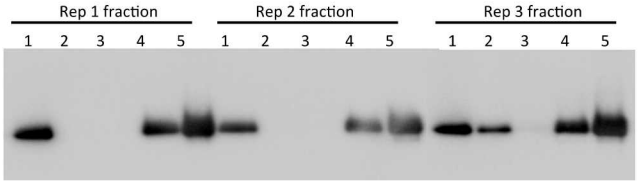

80:20 PC:PG					
4h incubation 20C, 6h spin 20C					
	Fraction 1	Fraction 2	Fraction 3	Fraction 4	Fraction 5
Rep1	0.92	0	0	0.72	1.00
Rep2	0.79	0	0	0.63	1.00
Rep3	0.82	0.36	0	0.67	1.00

Figure 4.11: Western blot of 12 mM sE + 80:20 PC:PG liposomes, incubated at pH = 3.0 for 4 hr at 20 °C. The mixture was then loaded onto a gradient and spun for 6 h at 20 °C.

4.2.2. Results

First we determined that for liposomes with composition PC:PG 70:30, E protein does not come off the membrane at an appreciable rate over the accessible temperature range after absorbing. We also determined that there is very little binding of sE to membranes of 100 % PC. So it was clear that an intermediate composition with %PG between 0 and 30% was needed. Therefore, the anchoring energy of sE was determined for liposomes with composition PC:PG 80:20. The fraction of bound protein remaining after various spinning times is plotted in Figure 4.12 for 20 ºC, 30 ºC and 40 ºC. The rate constants determined from the slopes of linear regressions are plotted in Figure 4.13 versus 1/T. The results indicate an activation energy of 188 kJ/mol corresponding to 60 kT at 37 ºC.

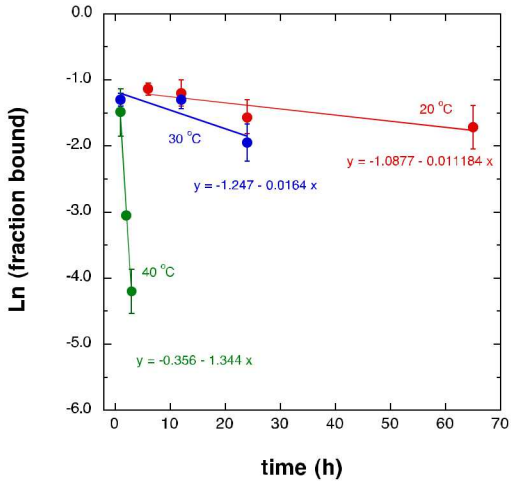

Figure 4.12: Fraction of protein bound to the liposomes as a function of time spinning at 54000 RPM at 20 °C, 30 °C, and 40 °C. The rate constants are given by the slopes of the lines.

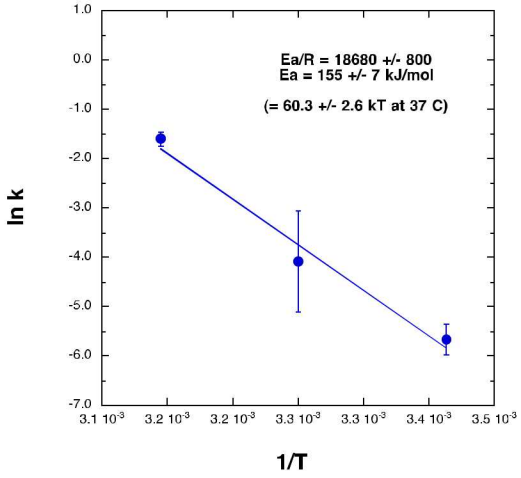

Figure 4.13: Arrhenius plot of the dependence of the rate constants on inverse temperature. The activation energy for unbinding is determined to be 155 kJ/mol from the slope. This corresponds to 60 +/- 3 kT at 37 °C.

4.3 Dependence of VLP binding on lipid composition

4.3.1. Method

The quartz crystal microbalance was used for measurements of the binding of VLPs to lipid bilayers, analogous to the measurements of sE binding to lipid bilayers. An important difference in protocol concerns the delay time between lowering the pH and injecting the solution into the measurement cell containing the SLB. This is important because the E protein on the surface of the VLPs undergoes a conformational change at low pH, and the hydrophobic fusion loop is exposed only for a limited time on the order of 10-20 minutes, after which it is thought to become buried into the lipid bilayer of the virus particle (Figure 1.5). Therefore, VLPs were typically added to the pH 5.5 buffer immediately prior to flowing the solution into the cell (10-15 s delay). For studies of the timescale of deactivation, the VLPs were added 10 min or 40 min prior to flowing the solution into the cell.

4.3.2. Results

Figure 4.14 shows results for wt VLPs of DV1 at 10.6 nM binding to PC:PG 70:30 and PC:PG 50:50 lipid bilayers. In each case a large excess of buffer was flushed through the measurement cell just prior to terminating the data collection to determine if the VLPs were bound irreversibly. For PC:PG 70:30 results are shown for pH 8 (control) and pH 5.5. For pH 5.5, results are shown for delay times of 10s, 10 min, and 40 min. The results show no detectable adsorption at pH 8, as expected. Comparing the results for PC:PG 50:50 with PC:PG 70:30, it is clear that the binding affinity is much greater for the bilayer containing 50% PG than for the bilayer containing 30% PG. Two curves are shown for a 10 s delay time and PC:PG 70:30 liposomes at pH 5.5. These show excellent reproducibility out to 50 min. The results for the different delay times show that the affinity is substantially reduced after a 10 min delay and strongly reduced after a 40 min delay. The frequency shift values for the two delay times ratioed to the values for a 10 s delay time are plotted in Figure 4.15 (left panel). These results indicate that more than half of the affinity is lost after a 10 min delay and 80% is lost after a 40 min delay at pH 5.5. We also measured the loss of affinity as a function of delay time at pH 6.0. Figure 4.15 (right panel) compares the loss of affinity for a 10 min delay time at pH 5.5 and pH 6.0. This is particularly relevant because the pH of the early endosome is estimated to be about 6.0 whereas that of late endosomes is pH 5.5. The results show that much less affinity is lost after a 10 minute delay time at pH 6.0 than at pH 5.5. This suggests that unbound DV does not inactivate during passage through early endosomes, where binding and fusion does not take place due to lack of AL.

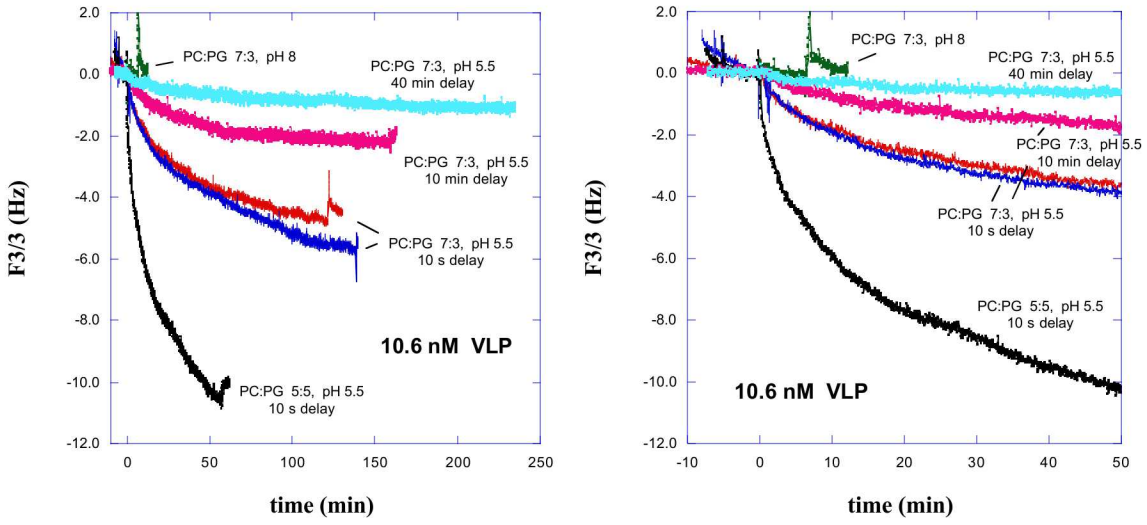

Figure 4.14. QCM data for VLP binding to PC:PG 70:30 lipid bilayers showing the effect of pH, mol% PG in the bilayer, and delay time between lowering the pH and injecting VLPs into the measurement cell containing the lipid bilayer. The right panel shows and expanded view of the first 50 minutes.

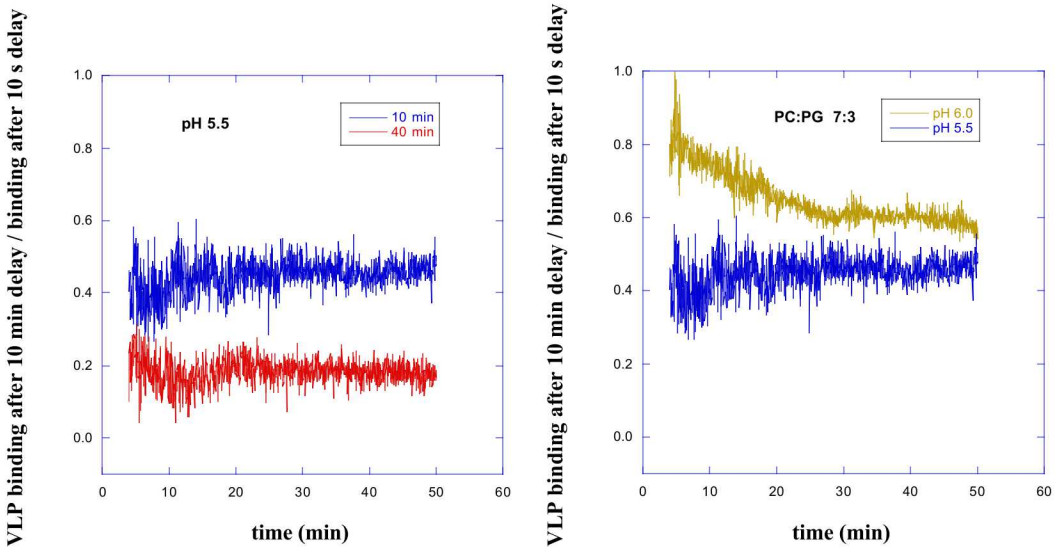

Figure 4.15: Loss of VLP binding as a function of delay time between lowering the pH and injecting the VLPs into the measurement cell. Left panel: VLP binding after 10 min and 40 min delay times relative to binding after 10 s delay time for VLP concentration of 10.6 nM and pH 5.5. Right panel: VLP binding after 10 min delay time relative to binding after 10 s delay time for pH 5.5 and pH 6.0.

Figure 4.16 shows QCM data for VLPs binding to PC:PG 70:30 and PC:PE:CH 49:21:30 lipid bilayers as a function of VLP concentration. For each case the delay time between lowering the pH and injecting the VLPs into the measurement cell was 10-15 s. The results show that the

binding affinity of VLPs for PC:PG 70:30 is 6-8 times greater than for PC:PE:CH 49:21:30 lipid bilayers. Since the binding affinity for free protein is a factor of two greater for PC:PG 70:30 than for PC:PE:CH 49:21:30, and assuming these values reflect the binding affinity of trimers, the results indicate that roughly 3-4 trimers bind per VLP. The maximum number of trimers on the VLP surface that could interact with a membrane is five, based on the geometry indicated by cryoEM imaging (ref). Therefore the value calculated here from comparing binding affinities for free protein and for VLPs is entirely reasonable. We note that the strong difference in binding affinity for the two membrane compositions could explain the lack of fusion in early endosomes as reported by Chernomordik group (ref). While that group attributed the lack of fusion to a difference in how the fusion loop inserts and also in the extent of trimerization, the large difference in binding affinity provides an alternative explanation.

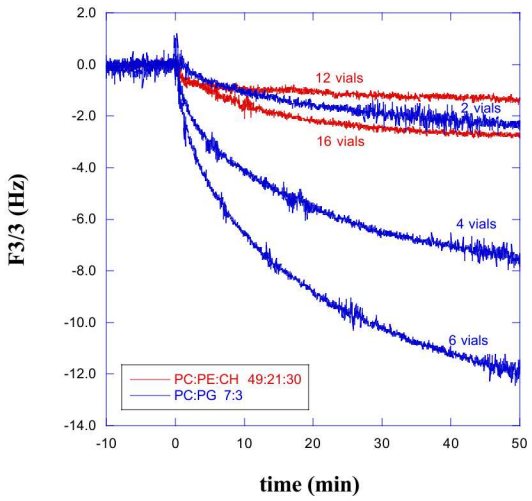

Figure 4.16: QCM data for VLP binding to PC:PG 70:30 and PC:PE:CH 49:21:30 lipid bilayers showing the effect of VLP concentration in each case. For each curve the delay time between lowering the pH and injecting VLPs into the measurement cell containing the lipid bilayer was ~ 10 s.

4.4 Dependence of VLP fusion on lipid composition

Fusion between VLPs and liposomes was assayed using the same protocol as reported by the Chernomordik group.[1] VLPs were incubated with a solution of the membrane dye DiD which incorporated into the VLP membrane to a level that resulted in self-quenching. Upon fusion, and more specifically upon mixing of the membranes of VLPs with liposomes, the dye is highly diluted, resulting in an increase in fluorescence. The most common method (method 1) to quantify the effect is to compare the fluorescence intensity to the value obtained after mixing the solution with the detergent Triton X at 0.1%. The latter is assumed to represent the 100% dequenched signal. However, that includes the intensity coming from VLPs that bound to liposomes as well as from VLPs that are free in solution. For tests involving different concentrations of VLPs, the % fusion value could decrease simply due to the increase in the 100% signal at higher concentrations of VLPs. So for such tests method 1 may not reflect the

relative amount of fusion that occurs with increasing concentration. Another way to quantify the effect (method 2) is to plot the increase in fluorescence during the measurement beginning immediately after lowering the pH. The advantage of this method is that the increase will only come from VLPs that are bound to liposomes and are fusing.

Figure 4-17 shows results for a test to optimize the DiD concentration. Figure 4-18 shows fusion results, quantified using method 1, for VLPs binding to PC:PG liposomes of various % PG. The fact that fusion continues to increase with %PG over the entire range suggests that fusion is limited by binding affinity of the VLPs. Note the strong correlation of these data with the binding data for sE in Figure 4.5. Figure 4.19 shows fusion data for PC:PE:CH 49:21:30, quantified using method 2. Figure 4.19 shows that fusion occurs with PC:PE:CH liposomes, but requires much higher concentration than for PC:PG 70:30. This is consistent with the conclusion that fusion is limited by binding affinity of the VLPs. In addition, fusion occurs more slowly with PC:PE:CH 49:21:30.

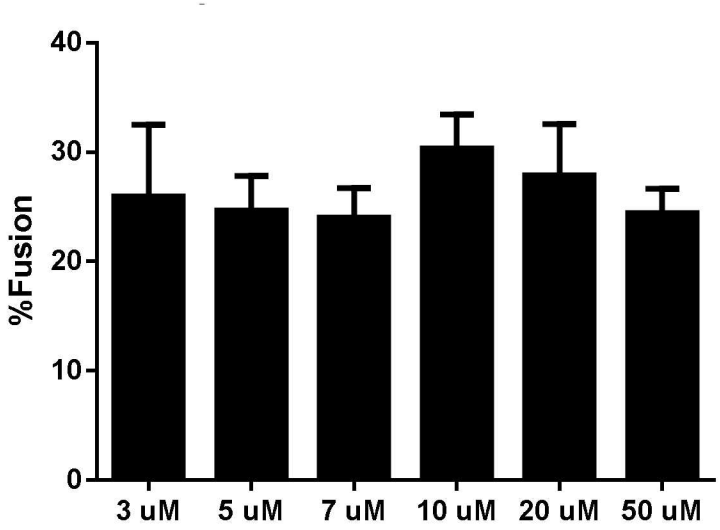

Figure 4.17: VLP-liposome fusion assay using DiD labeled VLPs. Optimization of DiD concentration.

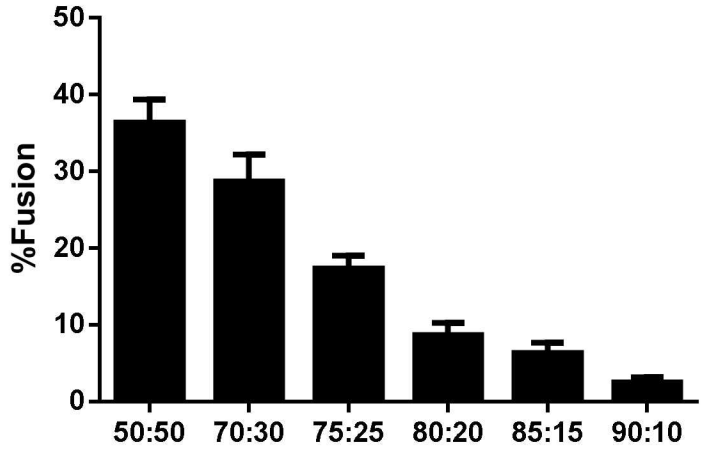

Figure 4.18: VLP-liposome fusion assay using PC:PG liposomes with a range of PG content.

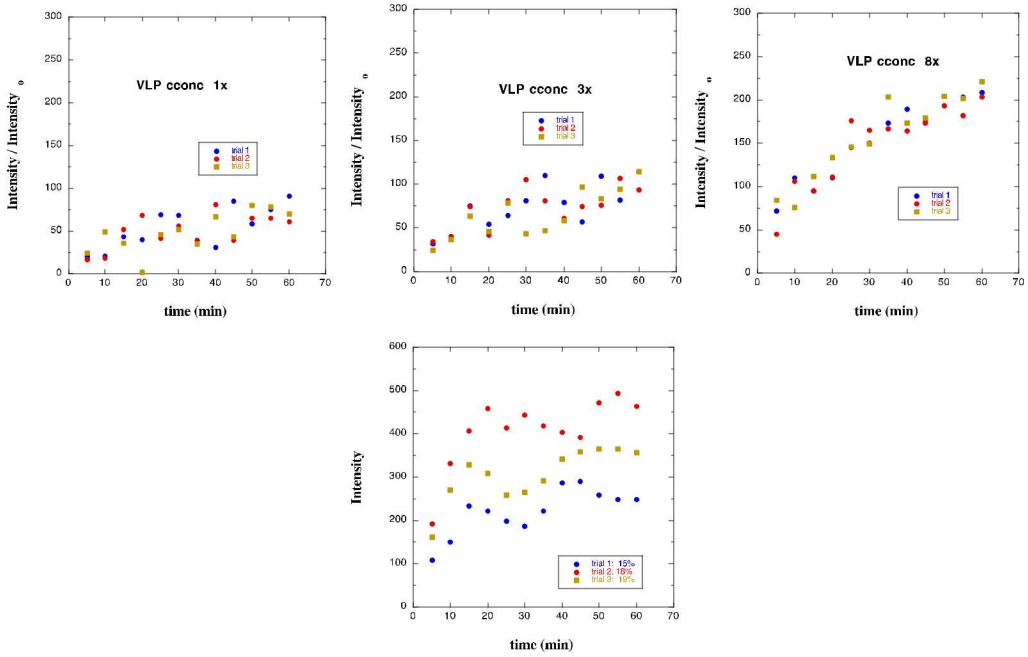

Figure 4.19: VLP-liposome fusion assay using PC:PE:CH 49:21:30 liposomes for concentrations 1x, 3x, and 8x that of the wt. Corresponding data for PC:PG 70:30 are shown in the bottom panel (note the change in the y-axis scale).

4.5 Dependence of VLP binding and fusion on mutations in the fusion loop

As described in the introduction, a great deal of evidence indicates that the sequence of the FL of DV is crucial for fusion. To perform tests on the role of mutations in the FL, we cloned the following mutations into VLPs: W101F, F108W, K110E. Then we tested binding to supported lipid bilayers by QCD and fusion to liposomes. Figure 4.20 compares binding of the different mutants to that for wt VLPs at approximately the same VLP concentration. The results suggest that binding is much weaker for the mutants than for the wt. However, the binding of the wt shows a lot of batch-to-batch variation, as shown in 4.20 (right panel). The origin of this variation is currently unknown, but could be related to varying levels of residual prM that remains bound to the VLPs during the maturation phase. Therefore, it is difficult to make firm conclusions regarding the relative binding levels of wt versus mutant VLPs. To resolve that, binding measurements over a wider concentration range are needed but are precluded due to a lack of sufficient amount of protein.

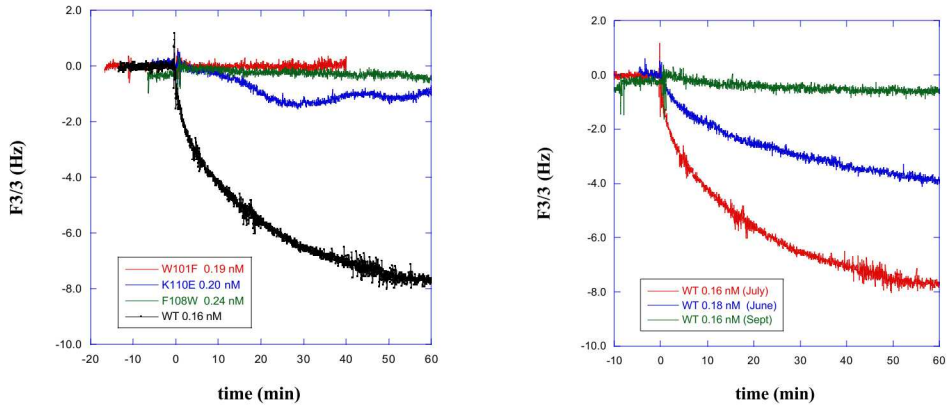

Figure 4.20: left panel: VLP-bilayer binding using PC:PG 7:3 liposomes and comparing wt and mutant VLPs. Right panel: VLP-liposome fusion assay using PC:PG 7:3 liposomes comparing wt VLPs from different batches.

In addition to binding measurements, we also performed fusion measurements of the mutant VLPs with liposomes. Figure 4.21 shows fusion results for W101F mutant VLPs with PC:PG 70:30 liposomes. Analogous data for the K110E mutant VLPs is shown in Figure 4.22. The legends indicate the % fusion values calculated by ratio to the intensity after Triton X addition. The results show that fusion does indeed occur for the mutant VLPs, indicating that those particular mutations in the fusion loop do not abolish fusion. However, fusion at the level observed for the wt only occurs at much higher VLP concentrations. When performed at the same concentration as for the wt VLPs in Fig 4.19, little or no fusion was observed. Figure 4.21 and Figure 4.22 show fusion data for mutant VLP concentrations that are 8x and 24x greater than for the wt VLPs in Figure 4.19. At 8x, little increase in fluorescence intensity occurs with time, which strongly suggests that little or no fusion occurs. However, when normalized to the intensity after addition of Triton X, the apparent % fusion is rather large. These two results are therefore in conflict. We believe that the lack of fluorescence increase with time over the first 20 min indicates that little fusion occurs, and that the relatively large intensities compared to that after Triton X addition are due to a large background signal rather than fusion. A large

background signal would occur, for example, if the DiD loading was lower in the mutant VLPs than in the wt VLPs. This is consistent with the visual appearance of the vials after labeling.

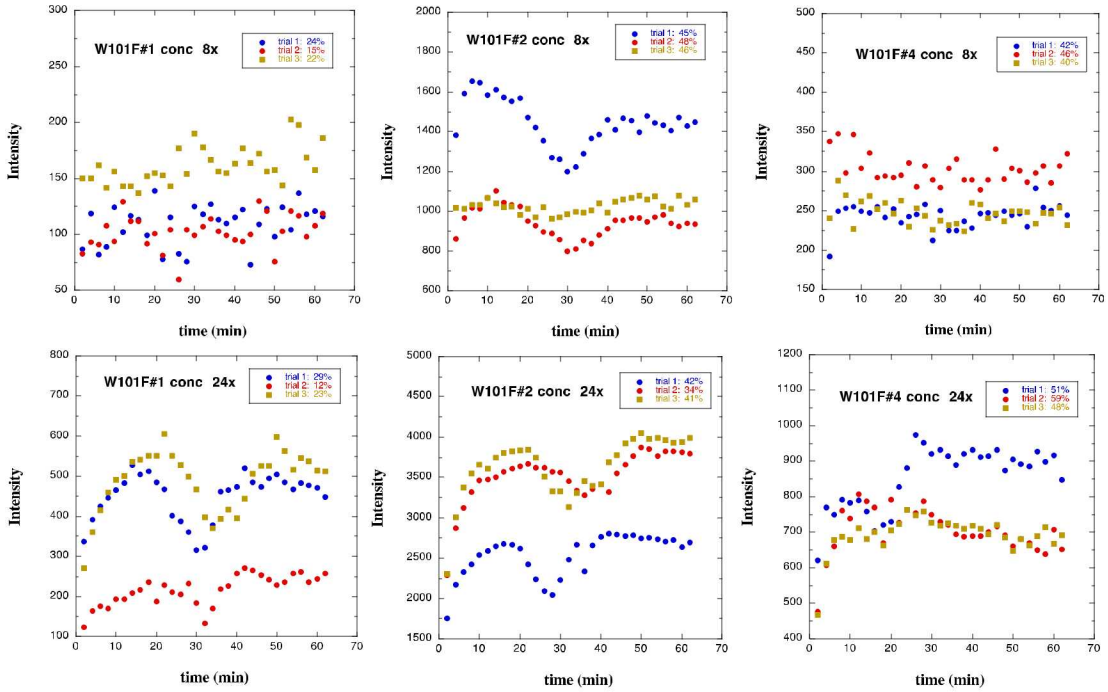

Figure 4.21: Fusion of W101F mutant VLPs with PC:PG 7:3 liposomes. Top panels: mutant VLPs at 8x of conc used for wt VLPs in Figure 4.19. Bottom panels: mutant VLPs at 24x of conc used for wt VLPs in Figure 4.19. The % fusion values obtained by ratio with the value after Triton X addition are given in the legends.

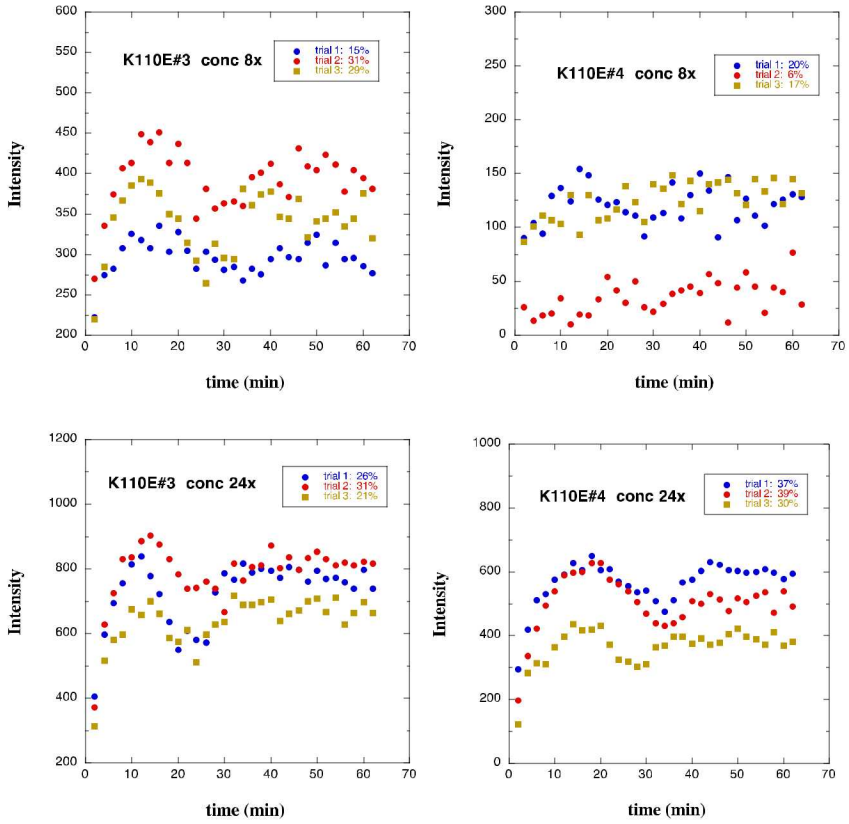

Figure 4.22: Fusion of K110E mutant VLPs with PC:PG 7:3 liposomes. Top panels: mutant VLPs at 8x of conc used for wt VLPs in Figure 4.19. Bottom panels: mutant VLPs at 24x of conc used for wt VLPs in Figure 4.19. The % fusion values obtained by ratio with the value after Triton X addition are given in the legends.

The results in Figure 4.21 and Figure 4.22 indicate that at 24x concentration of wt the extent of fusion occurs in the following order: W101F#4 > W101F#2 > W101F#1 and K110E#3 > K110E#4, although the difference is small between K110E#3 and K110E#4. The fact that fusion occurs with the mutant VLPs, but at much higher VLP concentration than for wt, suggests that the affinity for the membrane is reduced. Since the modeling results discussed below suggest that the mutations in the FL have little effect on the interactions that control binding and anchoring, we considered the possibility that residual prM may be present in the mutant VLPs that inhibits binding. To detect the presence of prM and to assess prM levels, western blots were run using an antibody that binds to prM. The results are shown in Figure 4.23 and Figure 4.24. Figure 4.23 shows a western blot of protein extracted from the mutant VLPs using an antibody for prM. The mutant VLPs are labeled at the top and free prM protein is shown at the right and used for calibration. The blot shows that substantial prM levels are indeed present. The results suggest that prM levels are in the following order: W101F#1 > W101F#2 > W101F#4 and K110E#3 >> K110E#4. The results suggest that very little prM is present in K110E#4. To control for varying concentrations, another blot was performed using the antibody for prM and also and antibody for domain III of E (far removed from the site of the mutations which is the FL located at the tip of domain II). The top bands are for the latter antibody, indicating relative concentration levels of E. The bottom bands are for the antibody for prM, indicating relative levels of prM present. Bands in Lanes 8 and 9 are for wt VLPs. The results in Figure 4.24 show the same relative levels of prM as mentioned above, and also shows that the prM levels for W101F#1, W101F#2, F108W#2, and K110E#3 are all greater than for wt.

While elevated levels of prM were indeed observed for some of the mutant VLPs, and the relative levels of prM correlate with the extent of fusion at the 24x concentration, the presence of prM alone does not appear to be sufficient to explain the fusion data. First, if the presence of prM alone is the cause of the lower binding affinity, then we would expect binding and fusion to occur at about the same level for W101F#4 and K110E#4 as for the wt, since the prM levels appear to be as low or lower for these mutants than for the wt. However, little or no fusion, as indicated by a strong increase in fluorescence with time over the first 20 min, was observed for these two mutant VLPs at a concentration comparable to that for wt. In fact, little or no fusion was observed for these mutant VLPs even at concentration 8x of wt. Second, very large differences in prM levels were observed for K110E#3 and K110E#4, whereas only a very small difference in fusion levels was observed. Finally, the prM level is greater for the wt batch from July than for the wt batch from Sept, and yet the binding results in Figure 4.20 indicate weaker binding for the wt batch from Sept. These facts suggest that most likely another factor is the cause of the primary adverse effect on affinity and fusion, and that prM level is likely to be only a secondary factor.

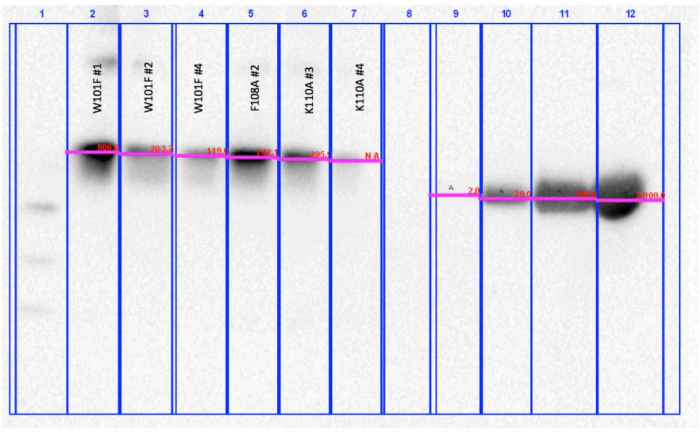

Figure 4.23: Western blot of protein extracted from the mutant VLPs using an antibody for prM. The mutant VLPs are labeled at the top and free prM protein is shown at the right and used for calibration.

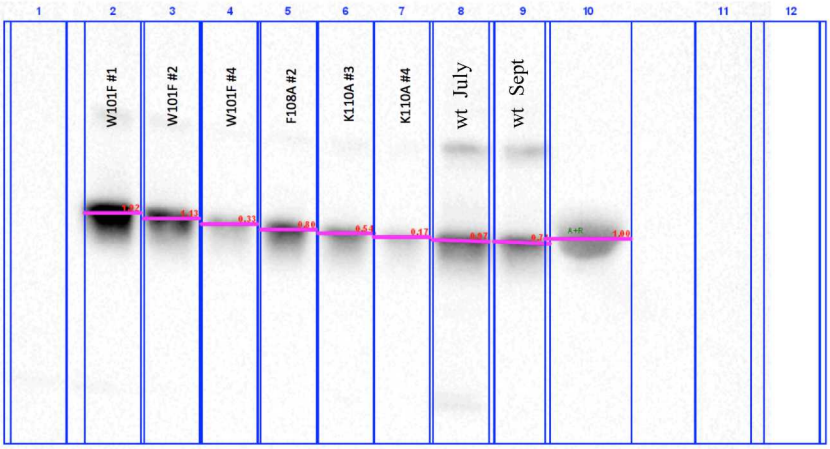

Figure 4.24: Western blot of E extracted from the mutant VLPs using the antibody for prM (lower bands) and also an antibody for E that binds to domain III far from the locations of the mutations (upper bands). Wt VLPs are shown at the right.

5. COMPUTATIONAL STUDIES

In this work we used molecular dynamics simulations run on Red Sky to understand how E protein catalyzes the fusion of the viral membrane to the endosome. The main goals of the computational and experimental work were to determine how different types of lipids modulate the behavior of the E protein, and how specific amino-acids near the tip of the protein interact with lipids to anchor E to the membrane. The simulation studies also tested the effects of mutations in the fusion loop. The results suggest that the fusion loop may play a role beyond simply anchoring E to the host membrane, such as facilitating lipid mixing between the two membranes by disturbing the host membrane structure.

While the experiments described earlier study the virus at the macroscopic scale, the simulations provide detailed and valuable information at the atomic scale. These details allow researchers to understand the molecular features responsible for membrane binding and anchoring, which may be invaluable in the development of vaccines and therapeutics to block fusion.

5.1 Combined all-atom simulation and continuum calculation of binding energy

Initially we performed a series of all atom simulations of sE timers interacting with PC:PG 70:30 and PC:PE:CH 1:1:1 lipid bilayers in which the distance of sE with respect to the membrane was varied. At each distance the simulation was run for 10 ns. The free energy at each position was determined relative to the system at large separation distance. For the PC:PG 70:30 lipid bilayer this resulted in a minimum in free energy when the FL was inserted 1.3 Å into the hydrophobic region of the lipid tails. This depth of insertion is in good agreement with the depth of insertion determined experimentally by NR. The free energy curve was put onto an absolute scale by comparison with continuum calculations involving electrostatic and dispersion interactions. The continuum calculations are valid until the protein and membrane come into direct contact, where the assumptions break down. No minimum in free energy was detected for the PC:PE:CH 1:1:1 lipid bilayers. This suggests a weaker interaction than with PC:PG 70:30, but is likely partially due to the lack of sufficient simulation time to allow for lipids to rearrange around the tip of sE. The full study is described elsewhere.[10]

5.2 Simulations of truncated sE binding to free and restrained lipid bilayers

The large size of the E trimer presents a barrier to the molecular modeling, as the computational cost of simulating the complete protein in the presence of a lipid membrane and solvent molecules is very large (system sizes on the order of a million particles). This is the reason that the abovementioned simulations were limited to 10 ns. We overcame this computational barrier by a dual approach where we adopted a more efficient united-atom interaction model, and also truncated the protein trimer while retaining its structural properties. By taking advantage of internal disulfide bonds near the tip region, the truncated sE trimer closely retains the structural features of the full sE trimer at a fraction of the computational cost.

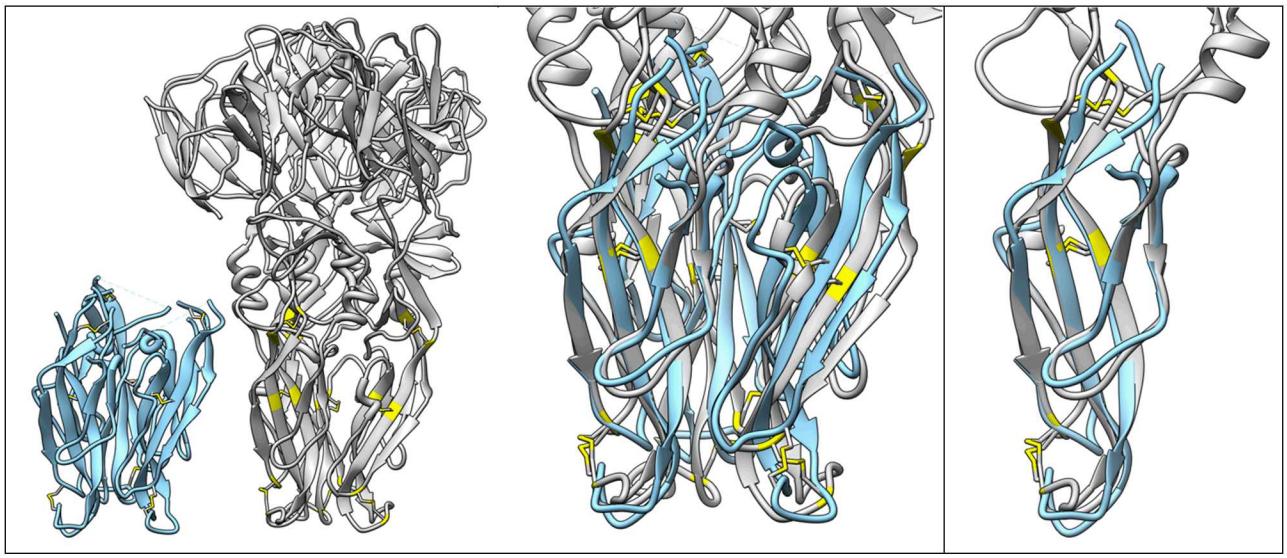

Figure 5.1: (Left panel) Side by side comparison of the truncated sE trimer (blue) and the full protein. (Middle) Overlap of the two protein structures after simulating each system for 100 ns. (Right) Structural alignment between the simulated truncated and full monomers. Disulfide bonds shown in yellow.

To investigate the effect of lipid composition on the interaction between the sE trimer tip and the membrane, we simulated the truncated protein system with a variety of lipid compositions. The membranes we tested include PC, PE, PG and cholesterol in various combinations. Our simulation setup consists of a membrane patch that is in contact with four truncated sE trimers (two on each side). The truncated E trimers were added to both sides of the membrane in order to compensate for any changes in the area or curvature of the membrane induced by the protein.

The results of simulations of several hundred nanoseconds show that the tip of the protein inserts in all the lipid compositions tested, in contrast to the 10 ns simulations sE with 1-1-1 PC:PE:CH bilayers discussed in section 5.1, with the hydrophobic loop residues coming into contact with the tails of the lipid molecules. As the protein inserts into the membrane, positively-charged lysine residues come into contact with the negatively charged oxygen atoms of the lipid phosphate group and form numerous hydrogen bonds. These interactions dominate and the hydrophobic interactions between the loop residues of E and the lipid membrane are of secondary importance. This is a major finding of this work. During the simulation there is a combination of tilting of the protein trimer and deformation of the membrane. The extent of the deformation appears to be correlated with the lipid composition, as different types of lipids change the elastic properties of the bilayer. This is a new finding not reported yet in the literature, and further work is required to determine if this plays a role in facilitating membrane fusion.

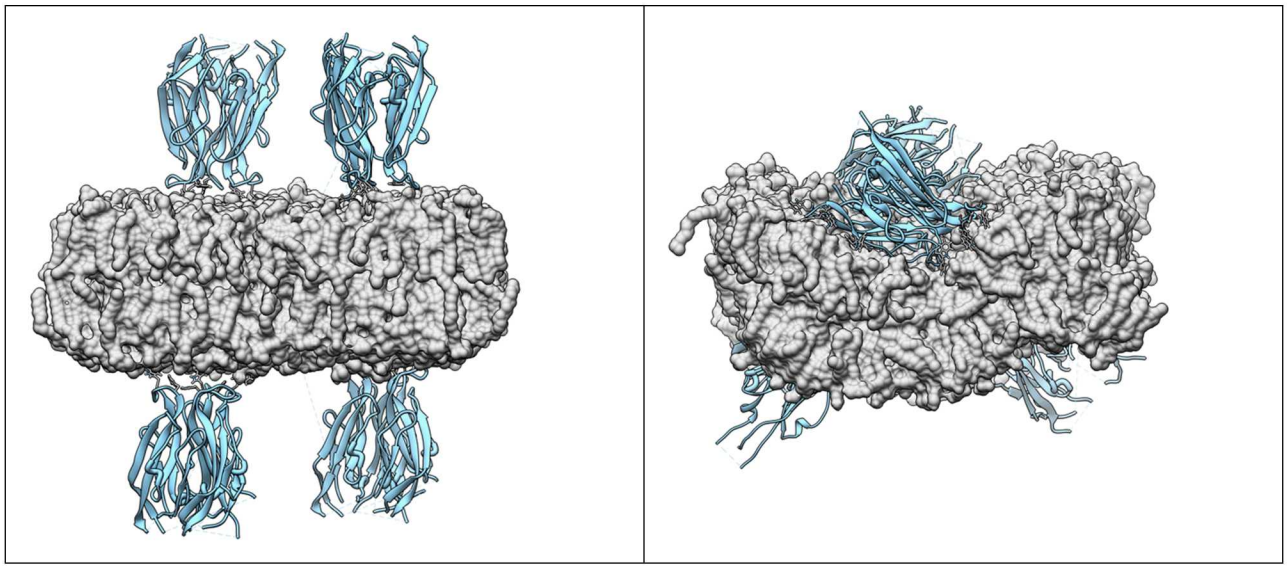

Figure 5.2: (Left) Starting configuration of a membrane simulation with four truncated trimers in contact with the lipid molecules. (Right) Snapshot of the system after simulating for 400 ns.

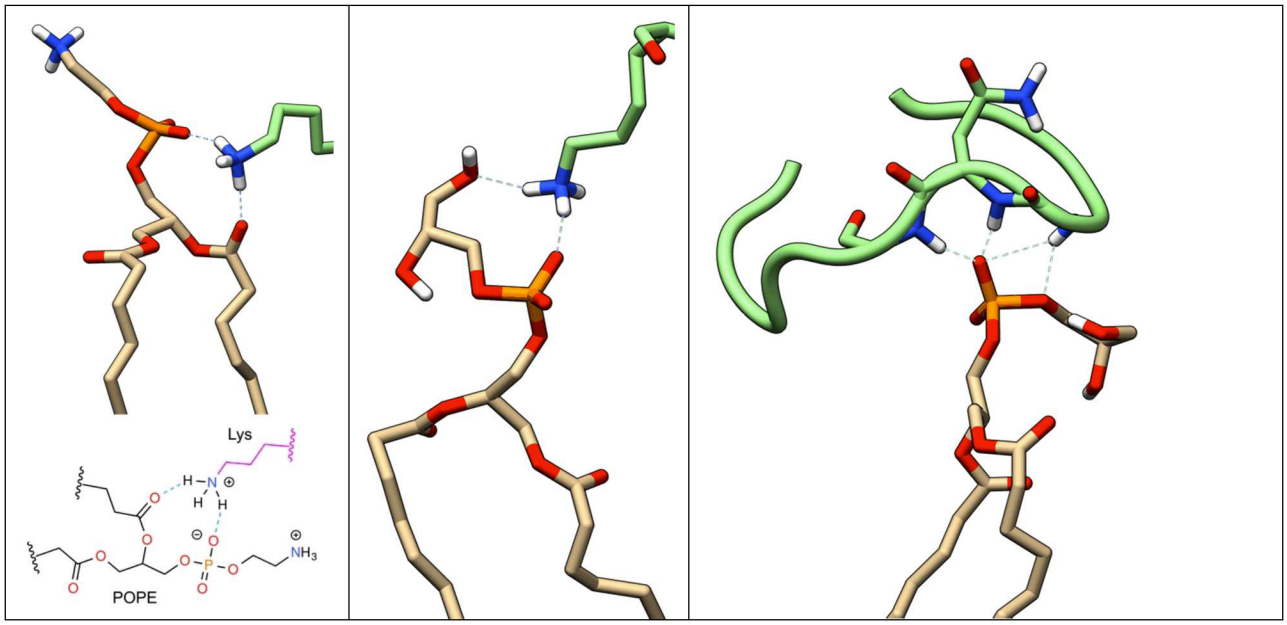

Figure 5.3: Different types of hydrogen-bonding interactions identified between the protein and lipid molecules.

We are currently in the process of quantifying the electrostatic interactions responsible for insertion and anchoring of the protein to the membrane, and to compare the strength of the interactions for membranes that contain anionic lipids (PG) or cholesterol. Also, we are analyzing the membranes and membrane-protein systems with continuum analysis tools to better understand the mechanical features of the lipid-protein interactions, which may provide some clues to understand the membrane fusion process.

In addition to simulations of the truncated wild-type protein, we have also conducted several simulations of the truncated protein with mutations in the fusion loop. This was motivated by the fact that others reported that fusion is severely attenuated by certain mutations in the fusion loop, such as W101F, F108W, and K110E (ref).[6,7] Our results to date show little difference in the interaction of the protein with the membrane due to these mutations, suggesting that specific residues in this part of the protein, which is highly conserved, do not play an important role in the anchoring. These mutations certainly do not inhibit insertion of the FL into the host membrane. This is another major finding of this work.

Finally, we are also testing a new methodology for simulating these membrane-protein systems with a restrained bilayer setup. In such a setup, the lipids in one layer of the membrane are restrained in the direction normal to the membrane plane using harmonic potentials, which in turn limit any deformation of the bilayer out of the plane. This was motivated by the desire to compare the simulations with the NR data of section 3.1, which involved a bilayer restrained by the substrate in a planar tethered geometry. These simulations constrain the out of plane deformation while allowing for expansion of the membrane within the plane and retaining fluidity. By restraining the bilayer out-of-plane fluctuations, we can more precisely compare the molecular features of the interaction (i.e., protein tilt and depth of insertion) with the NR results. The results show comparable depth of insertion and distribution of tilt angles as observed by NR for the two membrane compositions. The agreement is excellent for PC:PG 70:30. The simulations show a slightly (< 5 Å) deeper penetration in the case of PC:PE:CH and slightly larger tilt angle than for PC:PG 7:3. These differences may too small to resolve by NR.

The simulations that were conducted include:

- Full and truncated E protein trimer in solution without a membrane

- Truncated trimer of the wild-type protein with unrestrained membranes composed of:
    - PC
    - PC:PE 1:1
    - PC:PE:Cholesterol 35:35:30
    - PC:PG 70:30
    - PC:PE:PG 35:35:30
    - PC:PE:PG:Cholesterol 1:1:1, 30%

- Truncated trimer with mutations in the fusion loop, in contact with unrestrained membranes:
    - Single mutant W101F with PC:PG membrane
    - Single mutant F108A with PC:PG membrane
    - Single mutant K110E with PC:PG membrane
    - Double mutant W101F/F108A with PC:PG membrane

- Truncated trimer of the wild-type with restrained bilayers composed of PC:PG and PC:PE:Cholesterol

- Truncated trimer of mutants W101F/F108A and W101F with restrained bilayers composed of PC:PG

6. ATTEMPT TO DEVELOP A NEW FUSION ASSAY BASED ON FLOW CYTOMETRY

In addition to the DiD dequenching assay described in section 4.4, we also tried to develop a flow cytometry-based assay for VLP-liposome fusion based on light scattering detection of changes in liposome size distribution. This assay would provide a detection method that is entirely distinct from the DiD assay, and could also be used in high throughput. Using complimentary but orthogonal assays would greatly increase reliability.

The assay involves mixing the virus particles or VLPs with liposomes, lowering the pH of the solution and then analyzing the solution with a flow cytometer. To obtain a fluorescence readout, a fluorescent dye system must be incorporated into the membrane of either the VLP/virus or liposomal membrane that will report on lipid mixing or content mixing. In our work, we used the NBD-Rhodamine couple that self quenches at high loading in a membrane but then dequenches to give a FRET signal when diluted upon the lipid mixing stage of fusion.

Initial tests performed in SNL CA (Ryan Davis) involving POPC liposomes and POPG lipsomes. The flow-cytometer light scattering results showed an increase in scattering intensity for VLPs with POPG liposomes, indicating fusion, but no increase was observed for POPC liposomes. The light scattering readout is a measure of particle size. These studies thus show that the PG liposomes increase in size when fusion occurs with VLPs, and the size increase is large enough to be easily detected by light scattering in a typical flow cytometer. The light scattering signal was enhanced substantially by loading the liposomes with a contrast-enhancing agent. Likewise, the fluorescence readout indicated lipid mixing with POPG liposomes but not with POPC liposomes, correlating with the light scattering data. These results are shown in Fig 6.1. These promising initial studies were followed by extensive further studies involving PC:PG 70:30 liposomes, performed in SNL Albuquerque using the same type of flow cytometer by a technologist and student intern in collaboration with Ryan Davis. After > 1 yr of effort, the work was abandoned due to inability to reproduce results similar to those in Figure 6.1.

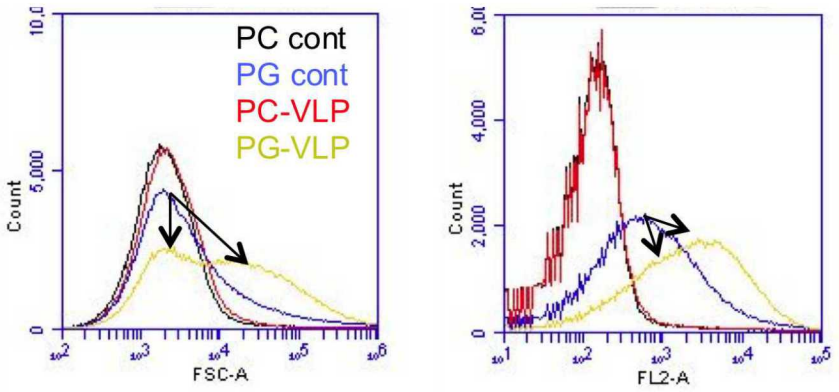

Figure 6.1: Light scattering (left panel) and fluorescence (right panel) readouts from a flow cytometer in initial fusion tests involving VLPs with POPC liposomes and POPG liposomes loaded with NBD-rhodamine.

7. ATTEMPT TO DEVELOP A VACCINE BASED ON THE FUSION LOOP

The following three sequences related to the beta-hairpin fusion loop peptide of the Dengue virus E protein were incorporated into an external loop of the M2 phage:

Fusion tip with S-S bond: FVCRHSFVDRGWGNGAGLFGKGGIVTCAK

Fusion tip without S-S bond: RHSFVDRGWGNGAGLFGKGGIVT

Conserved sequence only: DRGWGNGAGLFGKG

The highlighted sequence is ~ 99% conserved in flaviviruses. Expressing this sequence at the external loop of the M2 phage could yield VLPs that elicit an antibody response protective against Dengue virus. The work was performed by Carlee Ashley and Chris Lino. The first sequence has the advantage of a disulfide bond that staples the fusion loop into a hairpin conformation that should be very similar to that in the virus. However, the first two sequences listed above did not yield VLPs, as the sequences apparently disrupted the ability of the protein to fold correctly. The shortest sequence yielded VLPs. These VLPs raised high-titer peptide-specific antibody responses ($10^4 – 10^5$ titers after two immunizations). Further work is needed to determine if this response is protective. This work was not pursued because of funding limitations but also because it seems unlikely to be highly protective since the FL is only exposed in the endosome.

8. SUMMARY

In this work we develop unique experimental and modeling capabilities for studying virus-membrane interactions. We used these methods to test several important hypotheses. These are listed below along with the conclusions.

Insertion depth depends on lipid composition. The NR data and MD simulations both showed that E inserts into lipid membranes with compositions similar to those of plasma membrane/early endosomes (PM, no AL, 30% cholesterol) and late endosomes (LE, 30% AL). For both membrane compositions E inserts to a depth such that the FL is slightly inserted into the lipid tail groups. A small difference in depth of insertion ($\leq$ 5 Å) was indicated in the simulations, where a deeper insertion occurred with PM composition. This small degree of insertion is at the limit of what can be detected by NR. Both methods showed that E inserts at an angle, and that the preferred angular distributions were comparable for the two membrane compositions.

Five trimers per VLP interact with the host endosome membrane. Combining the data for the QCM binding measurements of the free protein and VLPs for the two membrane compositions indicates that 3-4 trimers interact with the endosomal membrane per VLP.

The affinity of E for the membrane is limiting. The QCM binding measurements (at < 1 nM VLPs) show a factor of 6-8 greater binding affinity for the LE composition compared with PM. So affinity is clearly important at such low concentrations. We estimate the concentration of VLPs in the endosome to be at about 20-30 nM and at this higher concentration it is possible that affinity is not limiting. We were unable to perform the QCM binding measurements at such high concentrations to directly test this hypothesis, due to insufficient quantity of VLPs. However, other results strongly suggest that affinity is limiting even at 20-30 nM. In particular at 20 nM VLPs, the fusion data showed a strong dependence on AL content from 0 - 50% that strongly correlates with E binding data for the same series. This observation, along with the facts that insertion of the FL and trimerization of E were shown to occur with both PM and LE compositions and that anchoring of E in the membrane was shown not to be limiting at 20% AL, suggests that affinity is indeed limiting and could explain why fusion of DV does not occur appreciably in early endosomes.

Anchoring of E in the membrane is not limiting. The new biophysical technique for measuring anchoring energy revealed an value of 60kT per trimer for PC:PG 80:20 membranes, or at least 180 kT per VLP. That value greatly exceeds the value of 50 kT estimated to be needed for membrane bending during fusion, and so we conclude that anchoring of E in the membrane is not limiting for the LE composition (30% PG). We were not able to complete a similar measurement for the PM composition. We note that the affinity of E for the PM composition exceeds that for 80:20 PC:PG, and so if that trend holds also for anchoring energy then anchoring energy will also not be limiting for PM composition. However, measurement of anchoring energy for the PM composition is needed to directly test the hypothesis for that case.

Trimerization of sE occurs upon membrane binding for both PC:PG 70:30 and PC:PE:CH 49:21:30 bilayers. However, due to limitations on the amount of protein available, we were

unable to study the time dependence of trimerization to determine if differences exist in the rate of trimerization.

Fusion only occurs appreciably when anionic lipids are present. The fusion data for liposomes containing cholesterol but no AL show that fusion occurs with PC:PE:CH 49:21:30 liposomes, but requires much higher concentration than for PC:PG 70:30. This is consistent with the conclusion that, in the case of PC:PE:CH 49:21:30 liposomes, fusion is limited by binding affinity of the VLPs. In addition, fusion occurs more slowly with PC:PE:CH 49:21:30. This interesting result suggests that rate of trimerization or physical properties of the membrane (membrane stiffness or lipid mobility) play a role.

The fusion loop plays a critical role other than anchoring E into the membrane. The MD simulations indicate that mutations in the FL (W101F, F108W, K110E) that have been reported to block fusion have very little impact on binding and certainly do not block binding and insertion of the FL. However, experimental studies on this topic were inconclusive.

The present work suggests a new therapeutic approach to blocking DV replication. Since fusion of DV occurs in endosomes, in contrast to viruses such as HIV or influenza where fusion occurs at the plasma membrane, developing a drug strategy to block fusion is substantially more challenging. In particular the fact that E rearranges from dimer to trimer while in the endosome, thereby exposing many possible drug targets only when in the endosome, presents a serious obstacle. Targeting a conformational change in E requires either that the drug make it into the endosome at sufficiently high concentration to bind to the target within a few minutes, or that the drug bind to a site on the mature virus (E in dimeric form, see Fig 1.1 and Fig 1.3) prior to entering the endosome that will also block the conformational change that leads to fusion. Therefore, blocking fusion by inhibiting conformational changes of E such as trimer formation, the rotation of domain III around domain I, and the association of the stem region with domain II to inhibit the zipping up process is very difficult (ref Harrison papers). Our work suggests that blocking the residues that are responsible for binding and/or anchoring of E to the endosomal membrane could be a promising alternative strategy. In particular the MD simulations showed that the interactions of E with the lipids are dominated by electrostatic interactions between lysines 246 and 247. The electron density map shown below indicates that these residues are exposed in the mature virus.

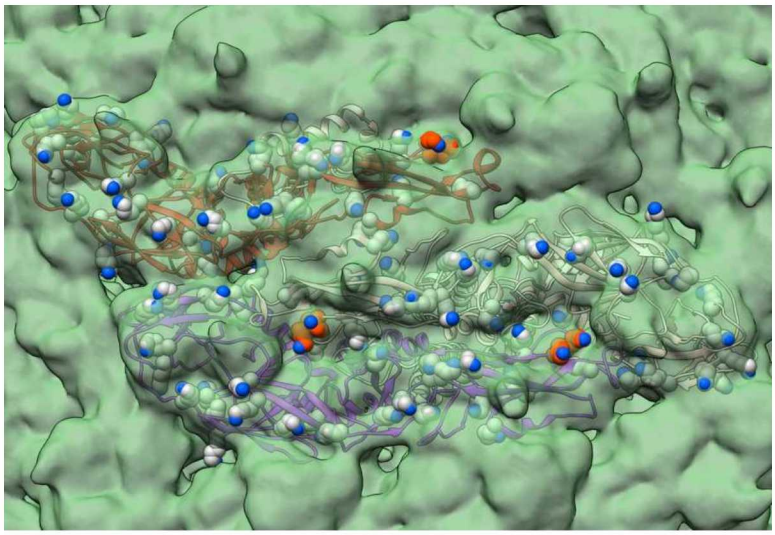

6. REFERENCES

(1) Zaitseva, E.; Yang, S.-T.; Melikov, K.; Pourmal, S.; Chernomordik, L. V. *PLoS Pathogens* **2010**, *6*, e1001131

(2) Stiasny, K.; Koessl, C.; Heinz, F. X. *Journal of Virology* **2003**, *77*, 7856.

(3) Lee, C.-J.; Lin, H.-R.; Liao, C. L.; Lin, Y.-L. *Journal of Virology* **2008**, *82*, 6470.

(4) Umashankar, M.; Sanchez-San Martin, C.; Liao, M.; Reilly, B.; Guo, A.; Taylor, G.; Kielian, M. *Journal of Virology* **2008**, *82*, 9245.

(5) Vashishtha, M.; Phalen, T.; Marquardt, M. T.; Ryu, J. S.; Ng, A. C.; Kielian, M. *J. Cell Biol.* **1998**, *140*, 91.

(6) Christian, E. A.; Kahle, K. M.; Mattia, K.; Puffer, B. A.; Pfaff, J. M.; Miller, A.; Paes, C.; Davidson, E.; Doranz, B. J. *Proc Natl Acad Sci U S A* **2013**, *110*, 18662.

(7) Huang, C. Y. H.; Butrapet, S.; Moss, K. J.; Childers, T.; Erb, S. M.; Calvert, A. E.; Silengo, S. J.; Kinney, R. M.; Blair, C. D.; Roehrig, J. T. *Virology* **2010**, *396*, 305.

(8) Modis, Y.; Ogata, S.; Clements, D.; Harrison, S. C. *Nature* **2004**, *427*, 313.

(9) Klein, D. E.; Choi, J. L.; Harrison, S. C. *Journal of Virology* **2013**, *87*, 2287.

(10) Rogers, D. M.; Kent, M. S.; Rempe, S. B. *BBA Biomembranes* **2014**, *in review.*

(11) Kasson, P. M.; Lindahl, E.; Pande, V. S. *PLoS Computational Biology* **2010**, *6*, e1000829.

(12) Larsson, P.; Kasson, P. M. *PLoS Computational Biology* **2013**, *9*, e1002950.

(13) Penfold, J.; Thomas, R. *J.Phys.: Condens.Matter* **1990**, *2*, 1369.

(14) Heinrich, F.; Ng, T.; Vanderah, D. J.; Shekhar, P.; Mihailescu, M.; Nanda, H.; Losche, M. *Langmuir* **2009**, *25*, 4219.

(15) Ganchev, D. N.; Rijkers, D. T. S.; Snel, M. M. E.; Killian, J. A.; de Kruijff, B. *Biochemistry* **2004**, *43*, 14987.

(16) Evans, E. *Faraday Discussions* **1998**, *111*, 1.

DISTRIBUTION

1	Michael S. Kent	8622 (electronic copy)	
1	Susan Rempe		8621 (electronic copy)
1	Bryan Carson		8622 (electronic copy)
1	Brianna Vernon	8621 (electronic copy)	
1	Juan Vanegas		8634 (electronic copy)
1	Sadie La Bauve	8622 (electronic copy)	
1	Dongmei Ye		8634 (electronic copy)
1	Ed Mozcydlowski		8634 (electronic copy)
1	MS0899	Technical Library	9536 (electronic copy)
1	MS0359	D. Chavez, LDRD Office	1911